DETECTION AND TRACKING OF DIM SIGNALS FOR UNDERWATER APPLICATIONS

A THESIS SUBMITTED TO
THE GRADUATE SCHOOL OF NATURAL AND APPLIED SCIENCES
OF
MIDDLE EAST TECHNICAL UNIVERSITY

BY

ESRA ŞENGÜN ERMEYDAN

IN PARTIAL FULFILLMENT OF THE REQUIREMENTS
FOR
THE DEGREE OF MASTER OF SCIENCE
IN
ELECTRICAL AND ELECTRONICS ENGINEERING

JULY 2010

Approval of the thesis:

DETECTION AND TRACKING OF DIM SIGNALS FOR UNDERWATER APPLICATIONS

submitted by **ESRA ŞENGÜN ERMEYDAN** in partial fulfillment of the requirements for the degree of **Master of Science in Electrical and Electronics Engineering Department, Middle East Technical University** by,

Prof. Dr. Canan Özgen ________
Dean, Graduate School of **Natural and Applied Sciences**

Prof. Dr. İsmet Erkmen ________
Head of Department, **Electrical and Electronics Engineering**

Prof. Dr. Mübeccel Demirekler ________
Supervisor, **Electrical and Electronics Engineering Dept., METU**

Examining Committee Members:

Prof. Dr. Kemal Leblebicioğlu ____________________
Electrical and Electronics Engineering Dept., METU

Prof. Dr. Mübeccel Demirekler ____________________
Electrical and Electronics Engineering Dept., METU

Assoc. Prof. Dr. Tolga Çiloğlu ____________________
Electrical and Electronics Engineering Dept., METU

Assoc. Prof. Dr. Çağatay Candan ____________________
Electrical and Electronics Engineering Dept., METU

Dr. Murat Şamil Aslan ____________________
TUBITAK UEKAE ILTAREN

Date: 13.07.2010

I hereby declare that all information in this document has been obtained and presented in accordance with academic rules and ethical conduct. I also declare that, as required by these rules and conduct, I have fully cited and referenced all material and results that are not original to this work.

Name, Last name : Esra ŞENGÜN ERMEYDAN

Signature :

ABSTRACT

DETECTION AND TRACKING OF DIM SIGNALS FOR UNDERWATER APPLICATIONS

Şengün Ermeydan, Esra
M.Sc., Department of Electrical and Electronics Engineering
Supervisor: Prof. Dr. Mübeccel Demirekler

July 2010, 86 pages

Detection and tracking of signals used in sonar applications in noisy environment is the focus of this thesis. We have concentrated on the low Signal-to-Noise Ratio (SNR) case where the conventional detection methods are not applicable. Furthermore, it is assumed that the duty cycle is relatively low. In the problem that is of concern the carrier frequency, pulse repetition interval (PRI) and the existence of the signal are not known. The unknown character of PRI makes the problem challenging since it means that the signal exists at some unknown intervals. A recursive, Bayesian track-before-detect (TBD) filter using particle filter based methods is proposed to solve the concerned problem. The data used by the particle filter is the magnitude of a complex spectrum in complex Gaussian noise. The existence variable is added in the design of the filter to determine the existence of the signal. The evolution of the signal state is modeled by a linear stochastic process. The filter estimates the signal state including the carrier frequency and PRI. Simulations are done under different scenarios where the carrier frequency, PRI and the existence of the signal varies. The results demonstrate that the algorithm presented in this thesis can detect signals which cannot be detected by conventional methods. Besides detection, the tracking performance of the filter is satisfying.

Keywords: Track-before-detect (TBD), particle filter, Gaussian, sonar

ÖZ

SUALTI UYGULAMALARI İÇİN ZAYIF İŞARETLERİN TESPİT VE TAKİBİ

Şengün Ermeydan, Esra
Yüksek Lisans, Elektrik Elektronik Mühendisliği Bölümü
Tez Yöneticisi: Prof. Dr. Mübeccel Demirekler

Temmuz 2010, 86 sayfa

Sonar uygulamalarında kullanılan sinyallerin gürültülü ortamda tespiti ve takibi bu tezin temel konusudur. Biz geleneksel tespit yöntemlerinin uygulanabilir olmadığı düşük Sinyal-Gürültü-Oranı (SNR) durumuna odaklandık. Dahası, doluluk-boşluk oranının göreceli olarak düşük olduğu varsayıldı. Söz konusu problemde, taşıyıcı frekansı, darbe tekrarlama aralığı ve sinyalin bulunup bulunmadığı bilinmemektedir. Darbe tekrarlama aralığının bilinmemesi durumu problemi daha da zorlaştırmaktadır çünkü bu durum sinyalin bazı bilinmeyen aralıklarla ortaya çıkması manasına gelmektedir. Problemi çözmek için, bir özyineli, Bayesian, parçacık süzgeç tabanlı yöntemleri kullanan tespitten önce takip süzgeci önerilmektedir. Parçacık süzgeci tarafından kullanılan veri kompleks Gauss gürültü içinde kompleks spektrumun büyüklüğüdür. Sinyalin varlığını belirleyebilmek için süzgecin tasarımına varlık değişkeni eklenmektedir. Sinyal durumunun evrimi doğrusal stokastik süreç ile modellenmektedir. Süzgeç, taşıyıcı frekansını ve darbe tekrarlama aralığını içeren sinyalin durumunu tahmin etmektedir. Sinyalin taşıyıcı frekansının, darbe tekrarlama aralığının ve sinyalin var olup olmadığı durumlarının değiştiği senaryolar altında benzetimler yapılmaktadır. Sonuçların gösterdiği gibi bu tezde sunulan algoritma geleneksel yöntemlerle tespit edilemeyen sinyalleri tespit edebilmektedir. Tespitin yanı sıra, süzgecin takip performansı beklentileri karşılamaktadır.

Anahtar Kelimeler: Tespitten önce izleme, parçacık süzgeci, Gauss, sonar

ACKNOWLEDGEMENTS

I am heartily thankful to my supervisor, Prof. Dr. Mübeccel Demirekler, for her professional guidance and suggestions throughout my thesis studies.

I would like to show gratitude to jury members Prof. Dr. Kemal Leblebicioğlu, Assoc. Prof. Dr. Tolga Çiloğlu, Assoc. Prof. Dr. Çağatay Candan and Dr. Murat Şamil Aslan for reviewing and evaluating my thesis.

I would like to thank TÜBİTAK UEKAE İLTAREN for deeply supporting my graduate studies. I also want to thank to my colleagues at work for their understanding and support during my academic studies.

I would like to express my deepest appreciation to my family, making me who I am now with their love, support and understanding throughout my life.

Finally, I wish to express my thanks to my husband, Ahmet Ermeydan, whose love, patience and trust encouraged me all the way. I would not have been pursued this research without him.

TABLE OF CONTENTS

ABSTRACT... iv
ÖZ v
ACKNOWLEDGEMENTS.. vi
TABLE OF CONTENTS vii
LIST OF TABLES ix
LIST OF FIGURES..x

CHAPTERS

1. INTRODUCTION 1

1.1 GENERAL INFORMATION...1
1.2 SCOPE OF THE THESIS 4

2. BACKGROUND 6

2.1 BAYESIAN ESTIMATION 6
2.1.1 Importance Sampling...7
2.1.2 State Space Representation...8
2.1.3 Particle Filter 9
2.1.4 Resampling Process...11
2.1.5 Selection of Importance Density 13
2.2 MONTE CARLO MARKOV CHAIN METHODS 15
2.2.1 Metropolis Hastings Algorithm 15
2.3 TRACK BEFORE DETECT (TBD) ALGORITHMS 16
2.3.1 Hough Transform...17
2.3.2 Dynamic Programming- Viterbi Algorithm...................................18
2.3.3 Particle Filter 19
2.3.4 Histogram PMHT 19

3. DETECTION AND TRACKING OF LOW SNR SIGNALS WITH TBD ALGORITHM...20

3.1 INTRODUCTION 20
3.2 SIGNAL MODEL 21
3.3 MEASUREMENT MODEL..22
3.4 PDF CONSTRUCTIONS OF THE PARTICLE FILTER 26
3.5 THE BAYESIAN FRAMEWORK APPROACH TO THE PROBLEM 27
3.5.1 The Signal State Density...28
3.5.2 Summary of the Derivations 30
3.6 PARTICLE FILTER IMPLEMENTATION 30
3.6.1 The PDF Representation of Continuous State: Existing Density......31
3.6.2 The PDF Representation of Continuous State: Birth Density...........32
3.6.3 The Probability of Existence..34

3.6.4 PRI Modeling 36
3.6.5 The Complete Algorithm 37
3.7 SIMULATIONS 44
3.8 THE PERFORMANCE OF THE ALGORITHM 59
3.8.1 Monte Carlo Simulations 60
3.9 CONCLUSIONS 66

4. FURTHER ANALYSIS OF THE PERFORMANCE OF THE FILTER .. 69

4.1 INTRODUCTION 69
4.2 SIMULATIONS 70
4.3 CONCLUSIONS 81

5. CONCLUSIONS 83

REFERENCES 85

LIST OF TABLES

TABLES

Table 2.1 Resampling Algorithm 12

Table 2.2 SIR Filter Algorithm..14

Table 2.3 Metropolis –Hastings Algorithm 16

Table 3.1 Particle Filter for Track-Before-Detect Algorithm...............................42

Table 3.2 Monte Carlo Simulation Parameters (A) 61

Table 3.3 Monte Carlo Simulation Parameters(B) 64

Table 4.1 Simulation Parameters for the First Experiment 71

Table 4.2 Simulation Parameters for the Second Experiment..............................77

LIST OF FIGURES

FIGURES

Figure 1.1 The signal in time domain 2

Figure 1.2 The signal in time domain where the carrier frequency is $fc = 20kHz$ and the signal is sampled at 50 KHz 3

Figure 1.3 The signal in time domain where the carrier frequency is $fc = 20kHz$ and the signal is sampled at 200 KHz 3

Figure 1.4 The entire simulated data with $\sigma_w{}^2 = 0.1$, the signal amplitude is $amp = 0.01$, the carrier frequency $fc = 20kHz$, the PRI $PRI = 1.5\sec$ and the pulse width $PW = 20\text{msec}$, the sampling frequency $fs = 50kHz$ 4

Figure 2.1 Hough Transform representation of range versus time [6] 18

Figure 3.1 The signal in time domain 25

Figure 3.2 The measurement frames, each corresponds to data of $0.5\sec$ 25

Figure 3.3 A priory distribution for the PRI values of the particles 36

Figure 3.4 The histogram of the samples obtained for PRI value 37

Figure 3.5 The simulated data with peak SNR 19.3 dB, the carrier frequency $fc = 20kHz$, the PRI $PRI = 1.5\sec$ and the pulse width $PW = 20\text{msec}$ 39

Figure 3.6 The measurement frames, each corresponds to data of $0.5\sec$ 39

Figure 3.7 The signal in time domain, the amplitude is $amp = 0.01$, the carrier frequency $fc = 20kHz$, the PRI $PRI = 1.5\sec$ and the pulse width $PW = 20\text{msec}$ 45

Figure 3.8 The entire spectrogram in noise 46

Figure 3.9 The measurement frames of $2nd$, $3rd$, $4th$ and $5th$ 46

Figure 3.10 The histogram of the carrier frequency of the particles 47

Figure 3.11 The carrier frequency component vs. the weights of the particles..... 48

Figure 3.12 The estimated carrier frequency vs. frame 49

Figure 3.13 The arrival time of the pulses 50

Figure 3.14 The probability of existence vs. frame 50

Figure 3.15 The signal in time domain, the amplitude is $amp = 0.008$, the carrier frequency $fc = 20kHz$, the PRI $PRI = 1.5\sec$ and the pulse width $PW = 20\text{msec}$ 51

Figure 3.16 The entire spectrogram in noise 52

Figure 3.17 The measurement frames of $2nd$, $3rd$, $4th$ and $5th$ 52

Figure 3.18 The histogram of the carrier frequency of the particles 53

Figure 3.19 The carrier frequency component vs. the weights of the particles 54

Figure 3.20 The estimated carrier frequency vs. frame 55

Figure 3.21 The arrival time of the pulses 56

Figure 3.22 The probability of existence vs. frame 56

Figure 3.23 The signal in time domain, the amplitude is $amp = 0.01$, the carrier frequency $fc = 20kHz$, the PRI $PRI = 1\sec$ and the pulse width $PW = 20\text{msec}$. 57

Figure 3.24 The entire spectrogram in noise 58

Figure 3.25 The measurement frames of $7th$, $8th$, $9th$ and $10th$ 58

Figure 3.26 The arrival time of the pulses 59

Figure 3.27 The average estimated carrier frequency over 50 simulations 62

Figure 3.28 The RMS error in carrier frequency over 50 simulations 62

Figure 3.29 The average probability of existence over 50 simulations 63

Figure 3.30 The average estimated carrier frequency over 50 simulations 65

Figure 3.31 The RMS error in carrier frequency over 50 simulations 65

Figure 3.32 The average probability of existence over 50 simulations 66

Figure 4.1 The signal in time domain, the amplitude is $amp = 0.01$, the carrier frequency $fc = 20kHz$ until time=6 sec and $fc = 10kHz$ after time=6.6 sec, the PRI $PRI = 1\sec$ and the pulse width $PW = 20\text{msec}$ 72

Figure 4.2 The measurement frames (peak SNR 9.79 dB) 73

Figure 4.3 The average estimated carrier frequency over 50 simulations 73

Figure 4.4 The RMS error in carrier frequency over 50 simulations 74

Figure 4.5 The average probability of existence over 50 simulations 74

Figure 4.6 The signal in time domain, the carrier frequency $fc = 20kHz$, the PRI $PRI = 1.5\sec$ until time=8sec and the $PRI = 2\sec$ until time=18sec 78

Figure 4.7 The measurement frames (peak SNR 9.79 dB)....................................78

Figure 4.8 The average estimated carrier frequency over 50 simulations.............79

Figure 4.9 RMS error in carrier frequency over 50 simulations............................79

Figure 4.10 The average probability of existence over 50 simulations.................80

Figure 4.11 The plot which demonstrates that PRI can be deduced from the probability of existence data..80

CHAPTER 1

INTRODUCTION

1.1 *General Information*

Detection and tracking are important subjects that are extensively studied in the literature. In this thesis, detection will mean deciding whether the received signal is emitted from a dynamic system such as radar, sonar etc. or simply represents the effects of interference which is referred as noise. Tracking is the process of extracting the information about the detected system such as its carrier frequency, pulse repetition interval etc. based on measurements. In the conventional approach, the detection and tracking is done by thresholding the output of a signal processing unit of a surveillance sensor [6].

However, the new technologies in electronics and the noisy environment that they placed harden the detection of enemy targets. The signals that are emitted from most of the radars and sonar have low duty cycle and these signals most of the time have low SNR (Signal to Noise Ratio).

The aim of this thesis is to detect and track constant PRI signals that are used in sonar applications. Since sonar applications are of our main concern we assume that computation of FFT is feasible so the frequency domain representation of the signal is used in detection and tracking. In our application we assume that the signal consists of a single sinusoid, so is narrow band and has a known duration. This framework may be considered as a restrictive one compared to detection and tracking of wide band signals like linear FM or non constant PRIs like staggered signals. However, the problem is interesting due to the challenge of detecting and tracking of very low SNR signals with relatively short duration. An example of the signal that we used in our experiments is given in Figure 1.1. The simulated data which will be used as the input to the filter is the magnitude of complex spectrum in complex Gaussian noise. The frequency domain representation of the signal in noise with peak SNR of 9.76 dB and average SNR of -8.96 dB, is given in Figure 1.4. The envelope of complex Gaussian noise is Rayleigh distributed and the magnitude of a signal in complex Gaussian noise is Ricean distributed [16]. Our aim is to detect and track this signal with low SNR. Since SNR is very low the problem will do the detection/tracking in Track Before Detect (TBD) sense. Furthermore because of the uncertainty of the existence of the signal as well as the uncertainty of the parameters of it we have modeled and solved the problem using particle filter. The Rayleigh characteristic of noise and the nonlinearity in the measurement model are also motives to prefer particle based filter.

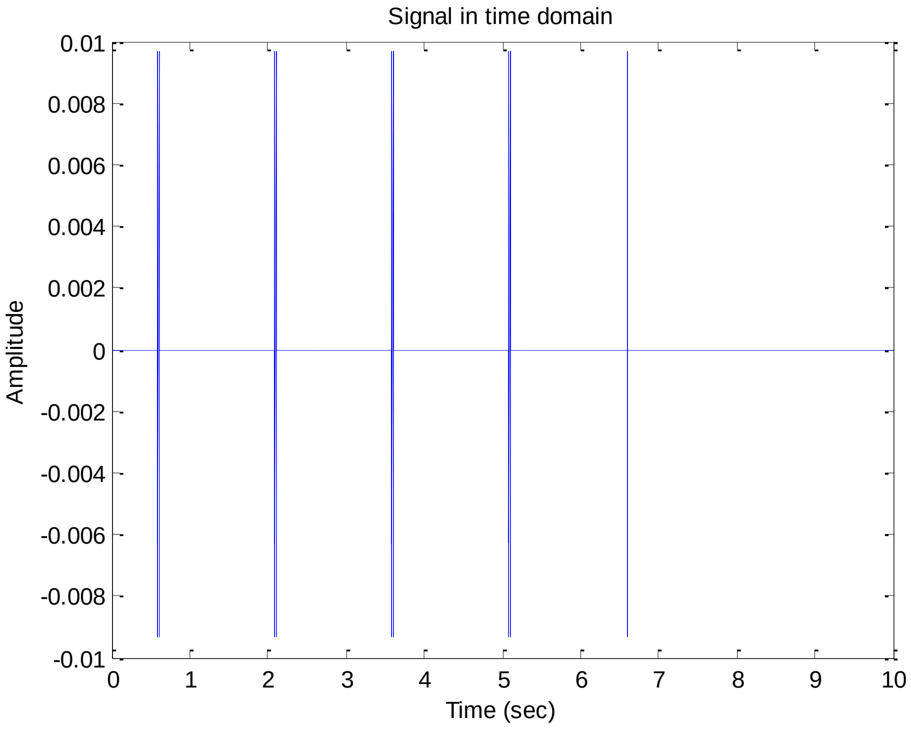

Figure 1.1 The signal in time domain

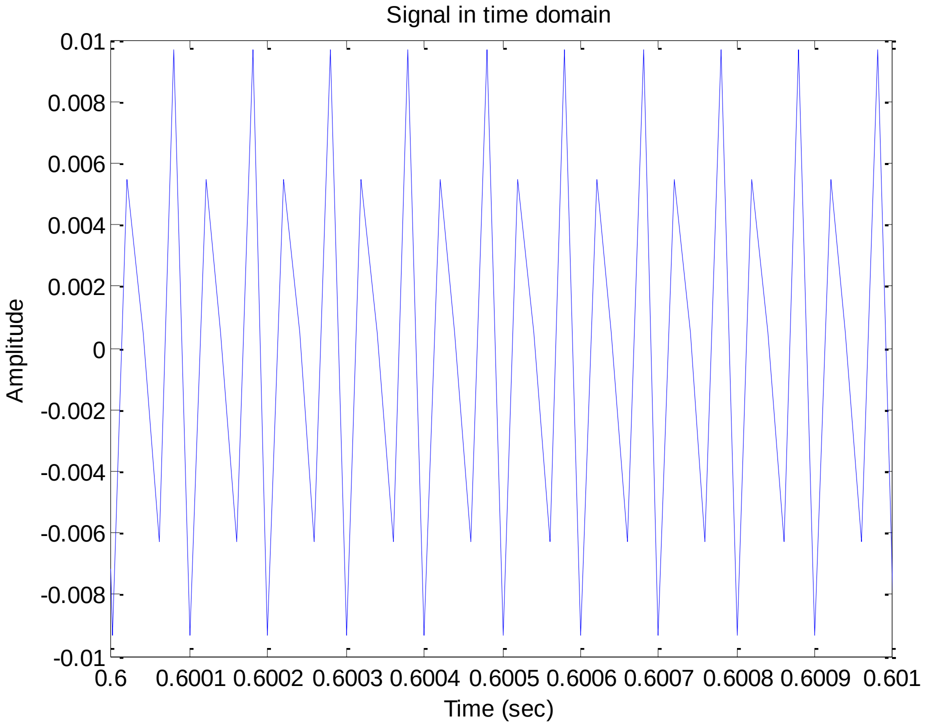

Figure 1.2 The signal in time domain where the carrier frequency is $fc = 20kHz$ and the signal is sampled at 50 KHz

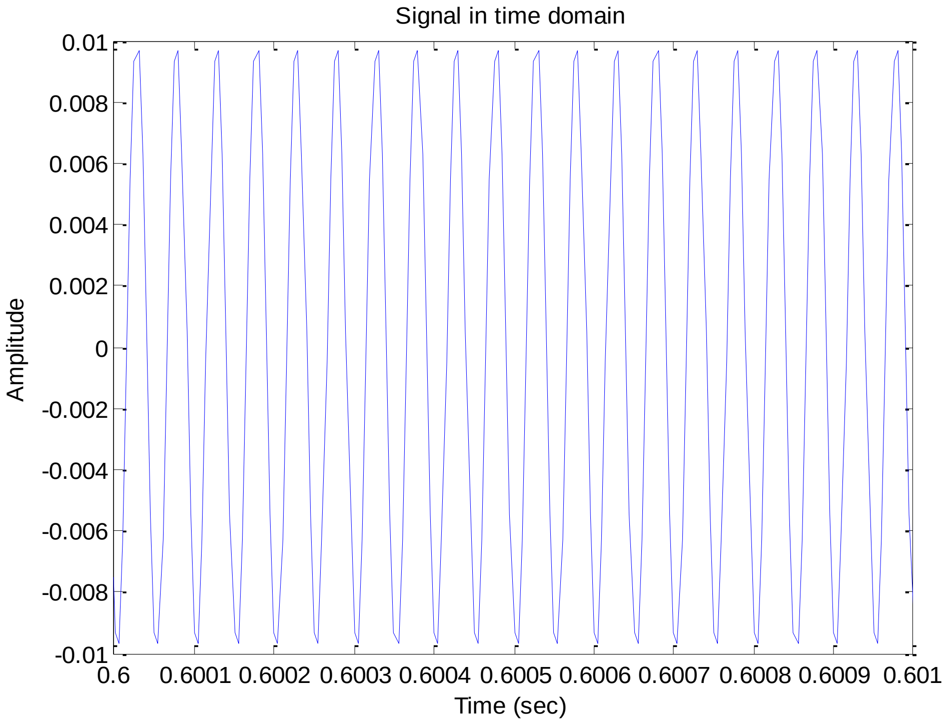

Figure 1.3 The signal in time domain where the carrier frequency is $fc = 20kHz$ and the signal is sampled at 200 KHz

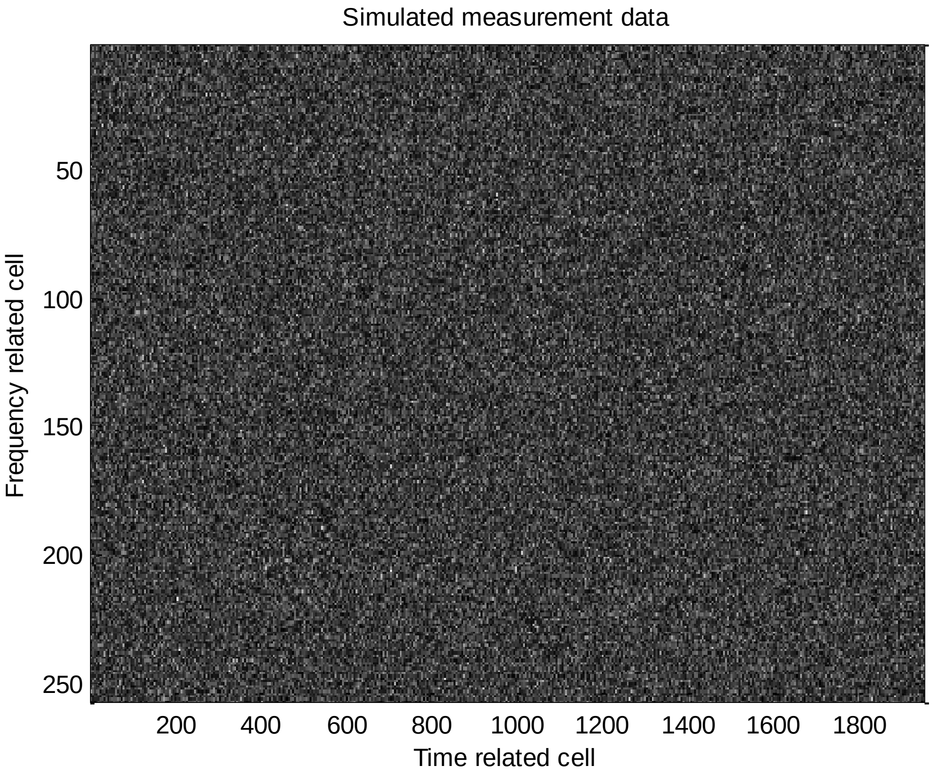

Figure 1.4 The entire simulated data with $\sigma_w{}^2 = 0.1$, the signal amplitude is $amp = 0.01$, the carrier frequency $fc = 20kHz$, the PRI $PRI = 1.5\sec$ and the pulse width $PW = 20\text{msec}$, the sampling frequency $fs = 50kHz$

1.2 *Scope of the Thesis*

In this study, a particle filter solution to low SNR signal detection and tracking is proposed. Proposed method is based on track-before-detect (TBD) approach. The thesis is composed of six chapters. In Chapter 2, the theoretical background of the particle filter and the track-before-detect algorithm is explained briefly.

In Chapter 3, the proposed particle filter based TBD algorithm is explained. The considered problem is that the carrier frequency, pulse repetition frequency (PRI) and the existence of the signal is not known. The thresholding process that is done in the conventional detection methods is not applicable since the aim is to detect low SNR signals.

In Chapter 4, the detection and tracking of signals emitting from frequency agile systems and PRI agile systems are investigated. Frequency agility is the ability to change the carrier frequency of the system; this technique is mainly used to account for jamming, and mutual interference with friendly sources. Some radars or sonar change their pulse repetition frequency (PRF), to benefit from the advantages of high and low PRF.

Conclusions that are obtained from this study and the future work are given in Chapter 5.

CHAPTER 2

BACKGROUND

2.1 *Bayesian Estimation*

A class of real world estimation problems is to get information about some parameter vector x given some observations y about that parameter vector. If there is some function that relates y to x such that $y = h(x)$, then the information about x can be deduced by using $x = g(y)$ where $g(y) = h^{-1}(y)$. This problem is known as parameter inversion (or parameter estimation) in the literature [1].

However in many practical situations, parameter (or state) vector x and observations are random quantities. For these cases the problem of making interference about x from observations y is solved by *Bayesian Estimation.* In the probability theory, any information about state x considering observations y is obtained by using:

$p(x \mid y)$: conditional probability density function (pdf) of x given y **(2-1)**

Probability density functions constitute a self-consistent mathematical modeling of the information about a parameter that allows making various inferences [4]. In the literature; mean, mode, median, and higher order moment estimates are used to extract a parameter given its pdf. The Bayes' theorem is used to obtain $p(x \mid y)$:

$$p(x \mid y) = \frac{p(y \mid x)\, p(x)}{p(y)} \qquad \textbf{(2-2)}$$

In this equation, the pdf $p(x \mid y)$ is also called the *posterior density* and $p(x)$ is called the *prior density*. The posterior density is used to represent what is known about x after the observation y. $p(y \mid x)$ is the conditional density of y given x and $p(y)$ is the marginal density of the observations and act as a normalization constant. $p(y)$ is calculated by the following expression:

$$p(y) = \int p(y \mid x) p(x) dx \qquad \textbf{(2-3)}$$

2.1.1 Importance Sampling

In many problems, the posterior density $\pi(x) = p(x \mid y)$ cannot be solved analytically. However, a numerical approximation can be obtained by using a large set of samples drawn from such a distribution; this approach is called *Monte Carlo (MC)* methods in the literature. Drawing samples from an arbitrary probability density function is generally not possible. So some sampling techniques are developed to overcome this difficulty. One of these sampling techniques is *importance sampling*. In this technique, another density $q(x)$ which is easy to generate independent samples from is used as *importance* or *proposal density.* The importance or proposal density should satisfy the following condition:

$$\pi(x) > 0 \Rightarrow q(x) > 0 \text{ for all } x \in R^{n_x} \qquad \textbf{(2-4)}$$

Then the Monte Carlo approximation for $\pi(x)$ with N samples is:

$$\hat{\pi}_N(dx) = \frac{\sum_{i=1}^{N} \omega(x^{(i)}) \delta_{x^{(i)}}(dx)}{\sum_{i=1}^{N} \omega(x^{(i)})} \qquad \textbf{(2-5)}$$

where $x^{(i)}; i = 1, \cdots, N$ are independent samples distributed according to $q(x)$ and $\omega(x^{(i)})$ are the importance weights defined as:

$$\omega(x^{(i)}) = \frac{\pi(x^{(i)})}{q(x^{(i)})} \qquad \textbf{(2-6)}$$

As it is seen the samples that should represent $\pi(x)$ are drawn from another density *q(x)* but are weighted according to the likelihood ratio values of them in two densities.

If the system is dynamic which means that the state x evolves with time, then the posterior density is represented as $\pi(x_k)$. In most of the situations, $\pi(x_{k+1})$ is calculated by using the new measurement and considering $\pi(x_k)$. In order to find samples which will be used to approximate $\pi(x_{k+1})$, samples of time k are recursively *re-weighted* based on measurement at time $k+1$. In the literature, the tools which use this procedure to estimate the posterior density sequentially and recursively as time evolves are called as *Particle filters*.

2.1.2 State Space Representation

The track-before-detect (TBD) problem which will be the focus of this thesis can be defined by considering the evolution of the state sequence $x_k, k \in N$ according to the following equation.

$$x_k = f_k(x_{k-1}, w_k) \qquad \textbf{(2-7)}$$

In this equation w_k, called process noise sequence, is a sequence of independent random variables with a known distribution. It is assumed that the initial state, state at $k=0$ has the prior density $p(x_0)$. Function f_k is assumed to be known. The objective is to recursively estimate the probability density function of the state x_k from the measurements. The relation between the state x_k and the measurement at time k defined as:

$$y_k = h_k(x_k, v_k) \qquad \textbf{(2-8)}$$

where v_k is a sequence of independent random variables with a known distribution called measurement noise sequence. h_k defines the measurement equation and is assumed to be known. The process and measurement noise sequences and the initial state are assumed to be independent.

2.1.3 Particle Filter

The discussion and derivations about the recursive particle filter given here is based on [2]. First of all, it is required to introduce the cumulative state and measurements up to time k as $X_k = x_j; j = 0,\cdots,k$ and $Y_k = y_j; j = 0,\cdots,k$. As it is mentioned earlier, Bayesian approach makes an interference about the state x_k, given the measurements up to time k. So the aim is to calculate the posterior distribution of x_k conditional on the measurements up to time k, i.e., $p(x_k | Y_k)$. The joint posterior density is denoted by $p(X_k | Y_k)$. $X_k{}^i, \omega_k{}^i\ {}_{i=1}^{N}$ denotes a set of weighted particles that characterizes the joint posterior $p(X_k | Y_k)$, where $X_k{}^i, i = 1,\cdots,N$ is a set of support points with the associated weights $\omega_k{}^i, i = 1,\cdots,N$. In this notation the weights are normalized such that $\sum_{i=1}^{N} \omega_k{}^i = 1$. If the Monte Carlo approach mentioned above is used, the joint posterior density is approximated as follows:

$$p(X_k | Y_k) \approx \sum_{i=1}^{N} \omega_k{}^i \delta(X_k - X_k{}^i) \qquad \textbf{(2-9)}$$

The normalized weights $\omega_k{}^i$ are chosen according to the principle of importance sampling which is mentioned before. If the samples $X_k{}^i$ are drawn from the importance density $q(X_k | Y_k)$, then according to (2-6):

$$\omega_k{}^i \propto \frac{p(X_k{}^i | Y_k)}{q(X_k{}^i | Y_k)} \qquad \textbf{(2-10)}$$

If at time step $k-1$ samples constituting an approximation to $p(X_{k-1} | Y_{k-1})$ are available, then as the measurement y_k is received at time k, $p(X_k | Y_k)$ can be approximated with a new set of samples. If the importance density is chosen to factorize such that:

$$q(X_k \mid Y_k) \;=\; q(x_k \mid X_{k-1}, Y_k) q(X_{k-1} \mid Y_{k-1}) \qquad \textbf{(2-11)}$$

then the samples $X_k{}^i \sim q(X_k \mid Y_k)$ can be obtained by including the new state $x_k{}^i \sim q(x_k \mid X_{k-1}, Y_k)$ to the existing samples $X_{k-1}{}^i \sim q(X_{k-1} \mid Y_{k-1})$. It is important to get the weight update equation. In order to derive that equation the distribution $p(X_k \mid Y_k)$ can be expressed in terms of the data likelihood and prior distribution:

$$\begin{aligned} p(X_k \mid Y_k) &= \frac{p(y_k \mid X_k, Y_{k-1}) p(X_k \mid Y_{k\text{-}1})}{p(y_k \mid Y_{k-1})} \\ &= \frac{p(y_k \mid X_k, Y_{k-1})\, p(x_k \mid X_{k-1}, Y_{k-1}) p(X_{k-1} \mid Y_{k-1})}{p(y_k \mid Y_{k-1})} \\ &= \frac{p(y_k \mid x_k) p(x_k \mid x_{k-1})}{p(y_k \mid Y_{k-1})}\; p(X_{k-1} \mid Y_{k-1}) \qquad \textbf{(2-12)} \\ &\propto p(y_k \mid x_k) p(x_k \mid x_{k-1})\; p(X_{k-1} \mid Y_{k-1}) \end{aligned}$$

Then using (2-11) and (2-12) in (2-10) , the weight update equation can be written as:

$$\begin{aligned} \omega_k{}^i &\propto \frac{p(y_k \mid x_k{}^i) p(x_k{}^i \mid x_{k-1}{}^i) p(X_{k-1}{}^i \mid Y_{k-1})}{q(x_k{}^i \mid X_{k-1}{}^i, Y_k) q(X_{k-1}{}^i \mid Y_{k-1})} \\ &\propto \omega_{k-1}{}^i \frac{p(y_k \mid x_k{}^i) p(x_k{}^i \mid x_{k-1}{}^i)}{q(x_k{}^i \mid X_{k-1}{}^i, Y_k)} \qquad \textbf{(2-13)} \end{aligned}$$

In many applications, it is only required to estimate $p(x_k \mid Y_k)$ in each time step, considering this the weight update equation can be modified as:

$$\omega_k{}^i \propto \omega_{k-1}{}^i \frac{p(y_k \mid x_k{}^i) p(x_k{}^i \mid x_{k-1}{}^i)}{q(x_k{}^i \mid x_{k-1}{}^i, y_k)} \qquad \textbf{(2-14)}$$

With the help of the modified weights the posterior density can be approximated as given in Equation (2-15).

$$p(x_k \mid Y_k) \approx \sum_{i=1}^{N} \omega_k{}^i \delta(x_k - x_k{}^i) \qquad \textbf{(2-15)}$$

Considering sequential measurements, the recursive propagation of the weights $\omega_k{}^i$ and support points $x_k{}^i$ the algorithm is defined as the Sequential Importance Sampling (SIS) particle filtering.

In the ideal case, the importance density function should be the posterior density itself. If the importance function of the form (2-11) is used, it has been shown that the variance of the importance weights can only increase over time [3]. This increase in variance decreases the accuracy and defined as *the degeneracy phenomenon* in particle filter. In real world applications, after a certain number of recursions, all but one particle will have extremely small normalized weights. A suitable measure of degeneracy of an algorithm is the effective sample size N_{eff} and estimated as [3]:

$$N_{eff} = \frac{1}{\sum_{i=1}^{N} (\omega_k{}^i)^2} \qquad \textbf{(2-16)}$$

where $\omega_k{}^i$ is the normalized weight obtained using (1.16). The value of N_{eff} lies in the interval $1 \le N_{eff} \le N$, so a small N_{eff} indicates severe degeneracy.

2.1.4 Resampling Process

In order to overcome the degeneracy of samples in SIS, resampling process is applied. Resampling is a crucial step in particle filtering algorithms when N_{eff} falls below a threshold N_{thr} which is predetermined [8]. The aim of the resampling process is to eliminate particles with low importance weights and replicate samples with high importance weights. Resampling involves a mapping of weighted particles $x_k{}^i, \omega_k{}^i$ into a new set of particles $\hat{x}_k{}^i, 1/N$ with uniform weights. Several resampling schemes have been proposed in the literature, the pseudo code of one of such resampling algorithms that is used in this thesis is given in Table 2.1.

Table 2.1 Resampling Algorithm

```
• Initialize the cumulative sum of weights(CSW): $c_1 = \omega_k{}^1$
• FOR $i = 2 : N$
    o Construct CSW: $c_i = c_{i-1} + \omega_k{}^i$
• End FOR
• Start at the bottom of the CSW: $i = 1$
• Draw a starting point $u_1 \sim U(0, \frac{1}{N})$ .
• FOR $j = 1 : N$
    o Move along the CSW: $u_j = u_1 + N^{-1}(j-1)$
    o WHILE $u_j > c_i$
        ▪ $i = i + 1$
    o END WHILE
    o Assign $\hat{x}_k{}^i = x_k$ and $\hat{\omega}_k{}^i = 1/N$ and obtain the resampled set
      $\hat{x}_k{}^i, 1/N$ .
• END FOR
```

2.1.5 Selection of Importance Density

One of the most critical issues in the design of the particle filter is the choice of the importance density $q(x_k \mid x_{k-1}{}^i, y_k)$. In this part, two standard choices are briefly explained.

The optimal importance density function that minimizes the variance of the importance weights, conditioned upon $x_{k-1}{}^i$ and y_k has shown to be [8] :

$$q(x_k \mid x_{k-1}{}^i, y_k)_{opt} = p(x_k \mid x_{k-1}{}^i, y_k)$$

$$= \frac{p(y_k \mid x_k, x_{k-1}{}^i) p(x_k \mid x_{k-1}{}^i)}{p(y_k \mid x_{k-1}{}^i)} \qquad \textbf{(2-17)}$$

Then the particle weights will be:

$$\omega_k{}^i \propto \omega_{k-1}{}^i p(y_k \mid x_{k-1}{}^i) \qquad \textbf{(2-18)}$$

If the optimal importance density function is used, the importance weights at time k can be computed before the particles are propagated to time k.

In order to use the optimal importance function, it must be possible to sample from $p(x_k \mid x_{k-1}{}^i, y_k)$ and evaluate $p(y_k \mid x_{k-1}{}^i)$. In the general case, either of these two may not be so easy [3].

In many applications, a suboptimal choice of importance function is used. The most popular suboptimal choice is the transitional prior:

$$q(x_k \mid x_{k-1}{}^i, y_k) = p(x_k \mid x_{k-1}{}^i) \qquad \textbf{(2-19)}$$

If the transitional prior is used as importance density function, then the importance weights are calculated as:

$$\omega_k{}^i \propto \omega_{k-1}{}^i p(y_k \mid x_k{}^i) \qquad \textbf{(2-20)}$$

It is mentioned that if the optimal importance density function is used, the importance weights at time k can be computed before the particles are propagated to time k. However, in the suboptimal choice computing the importance weights before the propagation of the particles is not possible. The pseudo code of the sequential importance resampling (SIR) filter algorithm is given in Table 2.2.

Table 2.2 SIR Filter Algorithm

```
Given the observed data $y_k$ at $k$ , do
• FOR $i = 1 : N$
    ○ Draw $x_k{}^i \sim p(x_k \mid x_{k-1}{}^i)$
    ○ Calculate $\tilde{\omega}_k{}^i = \frac{p(y_k \mid x_k{}^i) p(x_k{}^i \mid x_{k-1}{}^i)}{q(x_k{}^i \mid x_{k-1}{}^i, y_k)}$
• End FOR
• Normalize the weights: $\omega_k{}^i = \frac{\tilde{\omega}_k{}^i}{\sum_{j=1}^{N} \tilde{\omega}_k{}^j}$
• Calculate $N_{eff} = \frac{1}{\sum_{i=1}^{N} (\omega_k{}^i)^2}$
• IF $N_{eff} < N_{thr}$
    ○ Resample $x_k{}^i, \omega_k{}^i$ to obtain the new set of particles resampled set
      $x_k{}^i, 1/N$ .
• END IF
```

2.2 *Monte Carlo Markov Chain Methods*

Monte Carlo Markov Chain (MCMC) methods are used to simulate multivariate distributions using computer simulations. In MCMC, the goal is to construct a Markov Chain whose stationary distribution is the target density which is desired to simulate. (In Bayesian interference, the target density would typically a prior, $p(x)$, or a posterior $p(x|y)$, but MCMC can also be used in non Bayesian contexts.) In other words, MCMC methods can be used to get samples from target distribution using an easy-to-sample distribution. One of the algorithms used in this respect is Metropolis-Hastings algorithm.

2.2.1 Metropolis Hastings Algorithm

The details of the Metropolis-Hastings (MH) algorithm that is given here follow [5]. Consider a Markov Chain whose stationary distribution is the target density $\beta(x)$; x, x' are states in the chain. It is assumed that $q(x'|x)$ is candidate-generating density which is a function of both the current state x and the proposed state x'. The candidate-generating density should satisfy the following relation:

$$q(x'|x)\beta(x) > q(x|x')\beta(x') \qquad \textbf{(2-21)}$$

Then there will be a factor $r(x'|x) \leq 1$ such that the above relation is balanced:

$$q(x'|x)\beta(x)r(x'|x) = q(x|x')\beta(x') \qquad \textbf{(2-22)}$$

It is obvious that $r(x'|x)$ is obtained as:

$$r(x'|x) = \min\left\{1, \frac{q(x|x')\beta(x')}{q(x'|x)\beta(x)}\right\} \qquad \textbf{(2-23)}$$

The pseudo-code of the MH algorithm is given in Table 2.3.

Table 2.3 Metropolis –Hastings Algorithm

- Generate a candidate x' using $q(x' \mid x)$ and x.
- Evaluate the acceptance probability

$$\alpha = \frac{q(x \mid x')\beta(x')}{q(x' \mid x)\beta(x)}$$

$$r(x' \mid x) = \min \; 1, \alpha$$

  - Sample $u \sim U(0,1)$.
  - If $u \le r(x' \mid x)$, accept the move by seting $x = x'$, else reject it.

2.3 *Track Before Detect (TBD) Algorithms*

In traditional tracking algorithms, the measurements are extracted by thresholding the output of a signal processing unit of a surveillance sensor [6]. Thresholding reduces the data flow and thus simplifies the tracking process. The probability of target detection and the probability of false alarms are determined by the choice of the detection threshold for a target of a certain signal-to-noise ratio (SNR).

However, thresholding process can cause the elimination of the useful information. The loss of information is of little concern for high SNR targets, since good probability of detection can be achieved with a small false alarm rate. The development of the technology accelerated the implementation of low SNR targets such as stealthy military aircraft and cruise missiles. Using the unthresholded data for simultaneous detection and tracking of stealthy (dim) targets has a considerable advantage [7].

The concept of supplying the tracker with all of the sensor data without applying a threshold is known in the literature as *track-before-detect (TBD)* approach. TBD approach improves the track accuracy and gives opportunity to track low SNR targets. However, in TBD approaches the main difficulty is that the measurement is the whole sensor image so it is a highly nonlinear function of the target state. One way to overcome the problems is to discretise the state space. Several approaches for TBD have been developed using this method such as Hough Transform [6] , Bayesian estimator [9] and dynamic programming [7]. These methods operate on several scans of data, prohibit or penalize deviations from the straight-line motion; however using a discrete-state space in this approach requires enormous computational resources.

Particle filter approach is proposed to be an alternative to discretising the state. As it is explained in the previous sections, the particle filter is a tool which uses Monte Carlo techniques to solve the estimation integrals that are intractable. The application of particle filter to TBD problems are developed by a number of authors [2], [10] and [11].

Another approach to the TBD problems is the histogram probabilistic multihypothesis tracker, H-PMHT [12], [13]. The main difference between the H-PMHT and the other TBD algorithms is that H-PMHT uses a parametric representation of the target pdf rather than a numerical one. The computational load is reduced significantly in this approach [14].

In the following part, the brief information about the TBD algorithms is given.

2.3.1 Hough Transform

In Hough Transform, the measured data are transformed into stationary bins in target state space. The bins generally represent the two normal parameters of a straight line. Extensions to other types of curves have been made in the literature, however it can be stated that the Hough transform is most applicable to straight-line targets. In the application of Hough Transform to the TBD problems, the straight line to be detected defines the target range as a function of time and is given by:

$$\rho = R\cos\theta + t\sin\theta \qquad \textbf{(2-24)}$$

(2-24) represents a mapping form the time-range space to the Hough parameter space (ρ,θ). The target motion which defines a line in the time-range domain, can also be defined by two constant parameters in Hough domain. The parameters are the angle θ and the distance ρ from the origin to the line along the perpendicular shown in Figure 2.1 . (2-24) is used to compute a value of ρ for each θ_i. After a predetermined number of scans, detection is declared if the accumulated power exceeds a predetermined threshold in any (ρ,θ) bin. A detailed example of Hough Transform application to the TBD is given in [6].

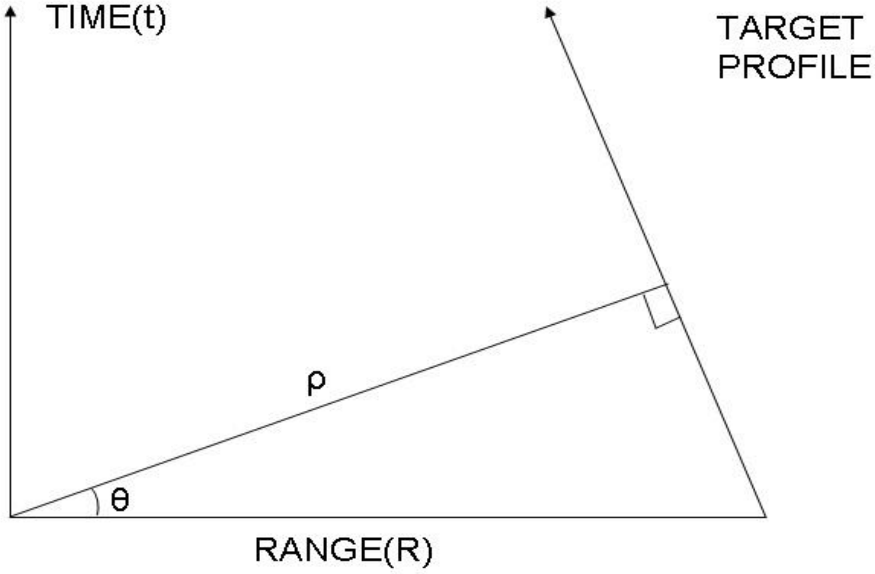

Figure 2.1 Hough Transform representation of range versus time [6]

2.3.2 Dynamic Programming- Viterbi Algorithm

As it is mentioned Hough Transform is mostly applicable to straight-line targets. The application of dynamic programming to TBD approach is more flexible and more readily available to maneuvering targets. Viterbi Algorithm (dynamic programming) is a maximum likelihood estimator for discrete states. The application of Viterbi algorithm to TBD is explained in [14]. The main task of the Viterbi algorithm is to find the most likely sequence of states. In other words, rather than accumulating the probability from alternate paths, Viterbi algorithm selects the single best path. One of the main advantages of this algorithm is that it always produces an estimate consistent with the dynamic model. However, it requires high computation.

2.3.3 Particle Filter

A recursive Bayesian filter incorporates the complete data as a highly non-linear measurement, which can be readily implemented using particle filter techniques. In the particle filter algorithm, a binary existence variable, E_k, is defined such that if $E_k = 0$ then there is no target; if $E_k = 1$, then target exists. The algorithm makes a direct approximation of the target-state posterior $p(x_k \mid E_k = 1, Y_k)$ and the existence probability $p(E_k \mid Y_k)$.

Two set of particles are constructed. The first set is the *birth particles,* they represent the case where the target did not exist in the data at time $k-1$ but it exists at time k; in other words the birth particles estimates $p(x_k \mid E_k = 1, E_{k-1} = 0, Y_k)$. The second is called *existing particles* and they represent the case where the target has continued to exist in the data from time $k-1$ to k. The existing particles are used to estimate $p(x_k \mid E_k = 1, E_{k-1} = 1, Y_k)$. The algorithm declares a target detected when the existence probability is above a tunable threshold. The details of the algorithm are given in [11], [14].

2.3.4 Histogram PMHT

In H-PMHT algorithm, the superposition of power from the scattering sources is assumed and the received power in each sensor pixel is probabilistically associated with the target and clutter models. For each model, the individual quanta and their assignment weights are combined to form a single synthetic measurement and measurement covariance. These measurement and covariance are used by point-measurement-based estimator. The application of H-PMHT to the TBD is detailed in [14].

CHAPTER 3

DETECTION AND TRACKING OF LOW SNR SIGNALS WITH TBD ALGORITHM

3.1 *Introduction*

In this thesis, a particle filter solution with track-before-detect (TBD) algorithm is used to detect signals that have low SNR. Particle filter based track-before-detect is developed in [10], [11] and [14]. However, all these works given in the literature are done for the purpose of tracking a dim target in an active way. The return signal exists at consecutive frames although it is very weak. The problem considered in this thesis is to detect signals in a very noisy environment for which the carrier frequency, pulse repetition interval (PRI) and the existence of the signal are not known. The unknown character of PRI makes the problem especially interesting since it means that the signal exists at some unknown intervals.

The thresholding process that is done in the conventional detection methods is not truly possible for low SNR signals. For low SNR targets the threshold must be low to allow sufficient probability of detection. However, a low threshold gives a high rate of false detections; following that the tracking system form false tracks. An alternative method is the track-before-detect algorithms where a threshold is not used. A recursive, Bayesian track-before-detect filter implemented using particle-based methods is the main focus of this thesis. The target existence and the measurements are modeled very similar to the models described in [11].

3.2 *Signal Model*

In the concerned detection problem, the threat signals are pulsed and their existence interval, carrier frequency, PRI and energy are not known. Besides, the duty cycles of the signals are quite low.

The signal state x_k consists of the carrier frequency fc_k, the Pulse Repetition Interval PRI_k, the power A_k and the time of arrival of the pulse tc_k. It is assumed that the time of arrival is related to the PRI of the signal. The evolution of the state is modeled by the linear stochastic process where $x_k = \ fc_k \quad PRI_k \quad A_k \quad tc_k \ ^{T}$:

$$\begin{bmatrix} fc_k \\ PRI_k \\ A_k \\ tc_k \end{bmatrix} = \begin{bmatrix} 1 & 0 & 0 & 0 \\ 0 & 1 & 0 & 0 \\ 0 & 0 & 1 & 0 \\ 0 & 1 & 0 & 1 \end{bmatrix} \begin{bmatrix} fc_{k-1} \\ PRI_{k-1} \\ A_{k-1} \\ tc_{k-1} \end{bmatrix} + w_k \qquad \textbf{(3-1)}$$

In this representation w_k is an independent, identically distributed Gaussian noise sequence with covariance matrix Q_k. The covariance matrix Q_k is assumed to be diagonal and in our application we have selected the covariance matrix as:

$$Q_k = \begin{bmatrix} 1 & 0 & 0 & 0 \\ 0 & 0.05 & 0 & 0 \\ 0 & 0 & 1 & 0 \\ 0 & 0 & 0 & 0 \end{bmatrix} \qquad \textbf{(3-2)}$$

The diagonal covariance matrix indicates uncorrelated noises for these quantities. Explanation about the selection of the values used in the covariance matrix is given in Section 3.6.1.

The existence of signal in the data is also determined by the system. The signal existence (presence) variable is represented by E_k where $E_k = 1$, if the signal is present, and $E_k = 0$ if there is no signal in the received data. The target existence is modeled by a two-state Markov chain. It is assumed that transitional probabilities of the Markov chain are defined in terms of signal's "birth" (P_b) and "death" (P_d) probabilities as:

$$\begin{aligned} P_b &= P \;\; E_k = 1 \,|\, E_{k-1} = 0 \\ P_d &= P \;\; E_k = 0 \,|\, E_{k-1} = 1 \end{aligned} \tag{3-3}$$

The probability of staying alive is represented by $1 - P_d$ and the probability of remaining absent is given by $1 - P_b$. The signal existence probabilities evolve according to:

$$E_k = \Pi E_{k-1} \text{ where } \Pi = \begin{bmatrix} 1-P_b & P_b \\ P_d & 1-P_d \end{bmatrix} \tag{3-4}$$

The initial target existence probability is assumed to be known.

'Time' is an important concept in this work. Discrete time is represented by a subscript k, however it may correspond to different real times for different particles that will be described later. To give better explanation for the time concept we will explain what actually is done during the process. The first step of the process is to take spectrogram of the signal for a time interval of τ_0 seconds. That will be considered as a 'measurement frame' of the system denoted as k at a nominal or the smallest possible time interval τ_0. The updating procedure of the filter by the measurement frame, however, is not done at each k but according to the value of the PRI of the particular particle of interest. The recursive filtering solution is explained in detail at section 3.5.

3.3 *Measurement Model*

One of the most common techniques for analyzing a given signal is Fourier Transformation. The frequency components of the signal can be examined via

Fourier Transform. For stationary signals, the Fourier Transform gives enough information about the frequency spectrum. However, most of the signals in real life have frequency contents that change over time. The most frequently used time-frequency representation of a signal is *Short-Time Fourier Transform (STFT).* In basic terms, STFT is a moving window Fourier Transform. The frequency content of a signal is examined as the time window is moved and a 2D time frequency distribution called *the spectrogram* is generated. As a result, the spectrogram gives information about the frequency content of the signal at different time instances [20].

The measurement model is based on the assumption that the sensor provides the spectrogram of the data in noise. The spectrogram of the data is obtained basically in two processes. Firstly, the signal is windowed and following that the discrete Fourier transform is applied. The measurement model uses the magnitude of the spectrum in each DFT bin. The entire spectrum obtained for a certain interval of length τ_0 is used as the measurement at discrete time k. As a result the measurement at time k is a matrix of size nxm where n is the number of frames that FFT is calculated in the time interval of length τ_0 and m is the number of frequency bins. Length τ_0 is selected considering the smallest possible value of PRI, since it is desired to have at most one pulse in one measurement frame.

Measurement is associated with the signal's state as well as the existence of it so its model is given in Equation (3-5). $y_k^{(i,j)}$ is the data at measurement frame k indexed by bin (i, j).

$$y_k^{(i,j)} = \begin{cases} \left| W^{(i,j)}(x_k) + V_k^{(i,j)} \right| & , if \;\; signal \;\; exists(E_k = 1) \\ \left| V_k^{(i,j)} \right| & , if \;\; signal \;\; does \;\; not \;\; exist(E_k = 0) \end{cases} \tag{3-5}$$

In (3-5), the function $W^{(i,j)}(x_k)$ represents the signal after the windowing and DFT process, $V_k^{(i,j)}$ denotes the background noise, $\left| \, . \, \right|$ denotes the magnitude. The central limit theory states that the background noise obeys a complex Gaussian distribution [4]. It is assumed that the background noise has zero mean or mean is subtracted. Therefore, $V_k^{(i,j)}$ is a zero mean identically and independently distributed complex random variable which is Gaussian with variance $2{\sigma_w}^2$.

The peak Signal to Noise Ratio (SNR) is defined as:

$$SNR = 10\log10\left(\frac{|W(x_k)|^2}{2{\sigma_w}^2}\right) \qquad \textbf{(3-6)}$$

The average Signal to Noise Ratio (SNR) is defined as:

$$SNR = 10\log10\left(\frac{|W(x_k)|^2}{2{\sigma_w}^2} \times \frac{PW}{PRI}\right) \qquad \textbf{(3-7)}$$

In the equation shown denoted as (3-7), PW and PRI represent the pulse width and the pulse repetition interval of the signal respectively.

In the track-before-detect applications considered in this thesis, the data forming the measurement, y_k, is the magnitude of the discrete Fourier transform of a windowed sinusoid in Gaussian noise. An example of the measurement frames used for simulations in this thesis is shown Figure 3.2 and the time domain representation of that signal is given in Figure 3.1. In Figure 3.2, the signal is circled in red. The peak SNR is 19.3 dB and the average SNR is 0.6 dB for this case. The smallest possible PRI is $0.5\sec$ in the simulations; therefore τ_0 is selected as $0.5\sec$.The distribution of the measurement data and the likelihood function are given in section 3.4.

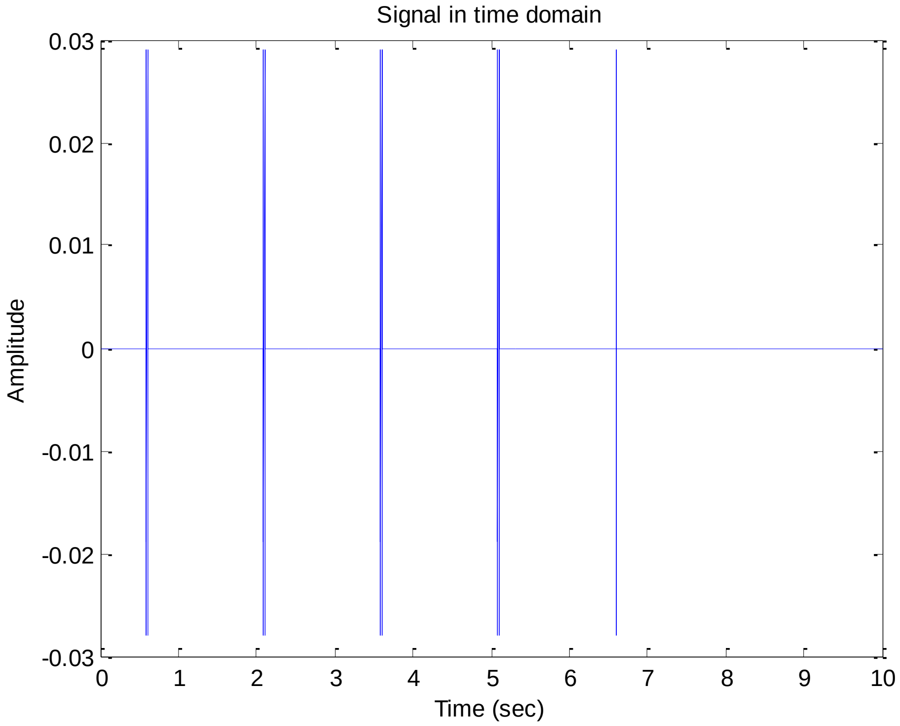

Figure 3.1 The signal in time domain

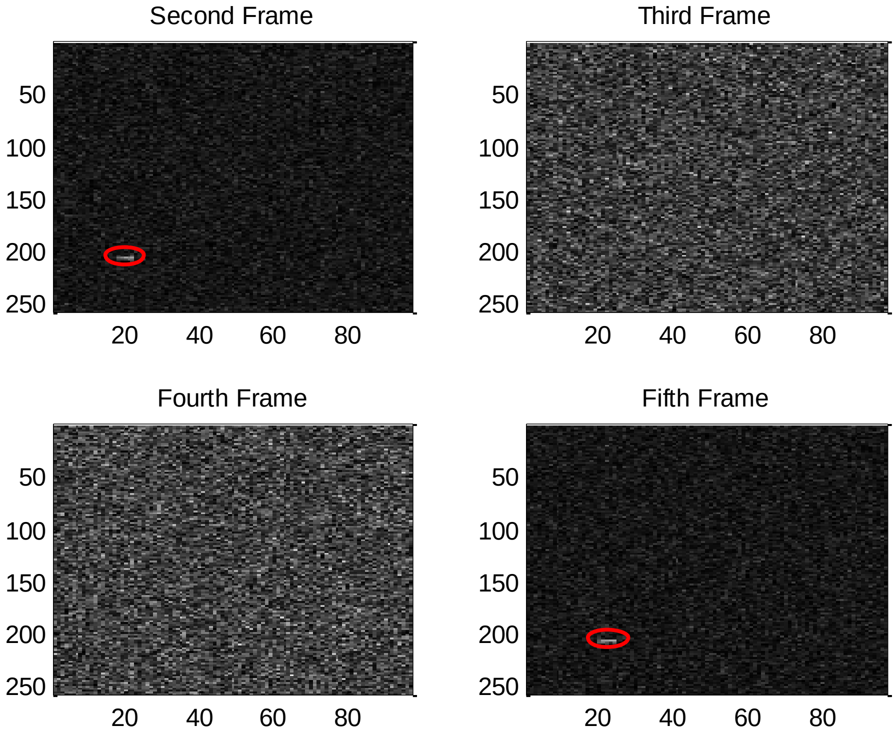

Figure 3.2 The measurement frames, each corresponds to data of 0.5sec

3.4 *PDF Constructions of the Particle Filter*

The distribution of the measurement data is modeled as explained in [16]. As it is stated, the measurement, y_k, is the magnitude of the discrete Fourier transform of a windowed sinusoid in Gaussian noise.

If there is a signal in the data, the intensity of each bin is Ricean distributed for which the likelihood function $p(y_k^{(i,j)} \mid x_k, E_k = 1)$ is expressed as in Equation (3-8).

$$\begin{aligned} &p(y_k^{(i,j)} \mid x_k, E_k = 1) \\ &= \frac{y_k^{(i,j)}}{\sigma_w^2} \times I_0\left(\frac{y_k^{(i,j)} \left|W^{(i,j)}(x_k)\right|}{\sigma_w^2} \right) \times \exp\left(-\frac{\left[y_k^{(i,j)}\right]^2 + \left[\left|W^{(i,j)}(x_k)\right|\right]^2}{2\sigma_w^2} \right) \end{aligned} \qquad \textbf{(3-8)}$$

where σ_w^2 is noise variance, $I_0(.)$ is the modified Bessel function of first kind and of order zero. The function $W^{(i,j)}(x_k)$ represents the signal after the windowing and DFT process, indexed by bin (i, j) and $|\ .\ |$ denotes the magnitude. The measured intensity in bin (i, j) is denoted by $y_k^{(i,j)}$.

If there is no signal in the data, in other words the data is only composed of noise, then the intensity in each bin is Rayleigh distributed. The density function of the Rayleigh distribution $p(y_k^{(i,j)} \mid E_k = 0)$ can be written as:

$$p(y_k^{(i,j)} \mid E_k = 0) = \frac{y_k^{(i,j)}}{\sigma_w^2} \times \exp\left(-\frac{\left[y_k^{(i,j)}\right]^2}{2\sigma_w^2} \right) \qquad \textbf{(3-9)}$$

The noise in each bin is assumed to be independent; therefore the complete density function is the product over all of the contributions from each bin.

$$p(y_k \mid x_k, E_k = 1) = \prod_{i=1}^{N}\prod_{j=1}^{M} p(y_k^{(i,j)} \mid x_k, E_k)$$

$$p(y_k \mid E_k = 0) = \prod_{i=1}^{N}\prod_{j=1}^{M} p(y_k^{(i,j)} \mid E_k) \qquad \textbf{(3-10)}$$

The likelihood ratio that will be used for the weights of the particles in the following sections is expressed as $l(y_k^{(i,j)} \mid x_k, E_k)$:

$$l(y_k^{(i,j)} \mid x_k, E_k) = \frac{p(y_k^{(i,j)} \mid x_k, E_k = 1)}{p(y_k^{(i,j)} \mid E_k = 0)} \qquad \textbf{(3-11)}$$

Using (3-16) and (3-15) $l(y_k^{(i,j)} \mid x_k, E_k)$ can be written as:

$$l(y_k^{(i,j)} \mid x_k, E_k) = \exp\left(-\frac{\left[W^{(i,j)}(x_k)\right]^2}{2{\sigma_w}^2} \right) \times I_0\left(\frac{y_k^{(i,j)} W^{(i,j)}(x_k)}{{\sigma_w}^2} \right) \qquad \textbf{(3-12)}$$

The complete likelihood ratio denoted as $L(y_k \mid x_k, E_k)$ is defined as:

$$L(y_k \mid x_k, E_k) = \frac{p(y_k \mid x_k, E_k = 1)}{p(y_k \mid E_k = 0)} \qquad \textbf{(3-13)}$$

$L(y_k \mid x_k, E_k)$ can be written as the product of the likelihood ratios in each bin:

$$L(y_k \mid x_k, E_k) = \prod_{i=1}^{N}\prod_{j=1}^{M} l(y_k^{(i,j)} \mid x_k, E_k) \qquad \textbf{(3-14)}$$

where the number of bins of data in the i and j directions are denoted as N and M respectively.

3.5 *The Bayesian Framework Approach to the Problem*

In this section, the problem of track-before-detect is formulated in the framework of recursive Bayesian estimation based on [11]. The aim is to find the joint posterior pdf at time k defined as $p(x_k, E_k \mid Y_k)$ and it is assumed that the latest data frame y_k and the joint posterior pdf of the signal state and the existence of the signal at time $k-1$, denoted as $p(x_{k-1}, E_{k-1} \mid Y_{k-1})$ is known. It should be reminded that Y_k denotes all the measurements from time 1 up to time k.

The aim of the track-before-detect filter is to find $p(x_k, E_k \mid Y_k)$ and the probability of existence $P(E_k = 1 \mid Y_k)$. The density denoted $p(x_k, E_k \mid Y_k)$ can be expressed as the product of two factors in Equation (3-15).

$$p(x_k, E_k \mid Y_k) = p(x_k \mid E_k, Y_k) P(E_k \mid Y_k) \qquad \textbf{(3-15)}$$

It is obvious that the state related with the signal x_k is undefined if $E_k = 0$, therefore in the calculation of the update equation, the density that is of concern will be $p(x_k \mid E_k = 1, Y_k)$.

In the calculation of $P(E_k \mid Y_k)$, the probability of existence $P(E_k = 1 \mid Y_k)$ and the probability of absence $P(E_k = 0 \mid Y_k)$ are related by:

$$P(E_k = 0 \mid Y_k) = 1 - P(E_k = 1 \mid Y_k) \qquad \textbf{(3-16)}$$

Therefore, it will be enough to calculate the probability of existence.

3.5.1 The Signal State Density

In this part, the signal state density denoted as $p(x_k \mid E_k = 1, Y_k)$ is derived. The signal state density can be approximated as:

$$p(x_k \mid E_k = 1, Y_k) \approx p(x_k \mid E_k = 1, E_{k-1} = 1, Y_k) + p(x_k \mid E_k = 1, E_{k-1} = 0, Y_k) \qquad \textbf{(3-17)}$$

In (3-17), the posterior state density is written as a sum of two densities. The first one denoted as $p(x_k \mid E_k = 1, E_{k-1} = 1, Y_k)$ is called the *existing* density where a signal existed in the data at time $k-1$. The density denoted as $p(x_k \mid E_k = 1, E_{k-1} = 0, Y_k)$ is called *birth* density where a signal has started to exist in the data between times $k-1$ and k.

The *existing* density $p(x_k \mid E_k = 1, E_{k-1} = 1, Y_k)$ can be expanded using Bayes' rule:

$$p(x_k \mid E_k = 1, E_{k-1} = 1, Y_k) = \frac{p(y_k \mid x_k, E_k = 1)\, p(x_k \mid E_k = 1, E_{k-1} = 1, Y_{k-1})}{p(y_k \mid E_k = 1, E_{k-1} = 1, Y_{k-1})} \quad \textbf{(3-18)}$$

If the numerator and denominator of the equation (3-18) are divided by $p(y_k \mid E_k = 0)$ which is the density when the signal does not exist, (3-18) can be expressed in terms of the likelihood ratio:

$$p(x_k \mid E_k = 1, E_{k-1} = 1, Y_k) = \frac{L(y_k \mid x_k, E_k = 1)\, p(x_k \mid E_k = 1, E_{k-1} = 1, Y_{k-1})}{L(y_k \mid E_k = 1, E_{k-1} = 1, Y_{k-1})} \quad \textbf{(3-19)}$$

The state dynamic model can be used in the calculation of the prediction density denoted as $p(x_k \mid E_k = 1, E_{k-1} = 1, Y_{k-1})$ in (3-19).

$$\begin{aligned} &p(x_k \mid E_k = 1, E_{k-1} = 1, Y_{k-1}) \\ &\quad = \int p(x_k \mid x_{k-1}, E_k = 1, E_{k-1} = 1)\, p(x_{k-1} \mid E_{k-1} = 1, Y_{k-1})\, dx_{k-1} \end{aligned} \quad \textbf{(3-20)}$$

The similar expansions are done in order to find the *birth* density:

$$p(x_k \mid E_k = 1, E_{k-1} = 0, Y_k) = \frac{p(y_k \mid x_k, E_k = 1)\, p(x_k \mid E_k = 1, E_{k-1} = 0)}{p(y_k \mid E_k = 1, E_{k-1} = 0)} \quad \textbf{(3-21)}$$

If the numerator and denominator of the equation (3-21) are divided by $p(y_k \mid E_k = 0)$ which is the density when the signal does not exist, then (3-21) can be expressed in terms of the likelihood ratio.

$$p(x_k \mid E_k = 1, E_{k-1} = 0, Y_k) = \frac{L(y_k \mid x_k, E_k = 1)\, p(x_k \mid E_k = 1, E_{k-1} = 0)}{L(y_k \mid E_k = 1, E_{k-1} = 0)} \qquad \textbf{(3-22)}$$

The prior density denoted as $p(x_k \mid E_k = 1, E_{k-1} = 0)$ describes the case where the signal has started to exist in the data between the times $k-1$ and k. (Note that if the target does not exist at the time $k-1$ then $p(x_k \mid E_k = 1, E_{k-1} = 0, Y_{k-1}) = p(x_k \mid E_k = 1, E_{k-1} = 0)$).

3.5.2 Summary of the Derivations

The terms that are derived in the preceding sections can be calculated as functions of

- the prior probability of existence, $P(E_{k-1} \mid Y_{k-1})$
- the Markov transition probabilities, P_b and P_d
- the likelihood ratio $L(y_k \mid x_k, E_k)$,
- a prior state density assuming that the signal existed at time $k-1$, $p(x_{k-1} \mid E_{k-1} = 1, Y_{k-1})$
- a transition density assuming that the signal continued to exist through times $k-1$ and k, $p(x_k \mid x_{k-1}, E_k = 1, E_{k-1} = 1)$
- a prior state density assuming that the signal started to exist between times $k-1$ and k, $p(x_k \mid E_k = 1, E_{k-1} = 0)$.

These quantities can be obtained from the state and the measurement models.

3.6 *Particle Filter Implementation*

The recursive Bayesian solution of the track-before-detect problem is based on *particle filtering*. A particle approximation is used to calculate and recursively update the posterior density $p(x_k \mid E_k = 1, Y_k)$. Each particle describes a possible state, x_k. Two sets of particles are used in the implementation of the particle filter and they are combined to form the posterior density. The first set of particles describes the existing density whereas the second set of particles describes the birth density.

3.6.1 The PDF Representation of Continuous State: Existing Density

This set of particles is used to approximate the density of the continuous state, $p(x_k \mid E_k = 1, E_{k-1} = 1, Y_k)$ when the signal exists. It is assumed that the prior density $p(x_{k-1} \mid E_{k-1} = 1, Y_{k-1})$ is represented by the set of particles $i \in 1....N_e$ called *existing particles* with values $x_{k-1}{}^{(e)i}$ and weights $\omega_{k-1}{}^{(e)i}$; N_e represents the number of existing particles. The algorithm of the calculation $p(x_k \mid E_k = 1, E_{k-1} = 1, Y_k)$ consists of the steps explained below:

1. The importance density is selected as transitional prior, i.e., $p(x_k \mid x_{k-1})$. With this choice the state transition model given in (3-1) is used to update the particles. The precise algorithm is given below by Equation (3-23). The particles representing state sequence is expanded according to this equation.

$$x_k{}^{(e)i} = \begin{bmatrix} 1 & 0 & 0 & 0 \\ 0 & 1 & 0 & 0 \\ 0 & 0 & 1 & 0 \\ 0 & 1 & 0 & 1 \end{bmatrix} x_{k-1}{}^{(e)i} + w_k{}^i \quad \forall i \in 1....N_e \qquad \textbf{(3-23)}$$

In Equation (3-23), w_k is an independent, identically distributed Gaussian noise sequence with covariance Q_k. The covariance matrix Q_k is given by:

$$Q_k = \begin{bmatrix} 1 & 0 & 0 & 0 \\ 0 & 0.05 & 0 & 0 \\ 0 & 0 & 1 & 0 \\ 0 & 0 & 0 & 0 \end{bmatrix} \qquad \textbf{(3-24)}$$

We assume that the noises affecting the state variables are independent. This assumption is reasonable for the first 3 state variables that correspond to carrier frequency, PRI and magnitude of the signal. The last state is the time of arrival of the signal which is clearly related with the PRI. We assume that the time of arrival is precise so it has no noise component but PRI, which can be considered as our sensing of the signal, is noisy. The values written as noise powers are somewhat arbitrary. The small value of the variance of PRI is a result of small intervals between possible PRI values.

2. The new particle weights are calculated using the likelihood ratio given in (3-14). The un-normalized weights denoted as $\omega u_k^{(e)i}$ are calculated as:

$$\omega u_k^{(e)i} = \frac{1}{N_e} L(y_k \mid x_k^{(e)i}, E_k) \;\; \forall i \in \; 1....N_e \qquad \textbf{(3-25)}$$

3. The weights are normalized:

$$\omega_k^{\;i} = \frac{\omega u_k^{\;i}}{\sum_{n=1}^{N} \omega u_k^{\;n}} \;\; \forall i \in \; 1....N \qquad \textbf{(3-26)}$$

4. The approximation for the posterior density $p(x_k \mid E_k = 1, E_{k-1} = 1, Y_k)$ is obtained by using the set of particles $x_k^{(e)i}$ with the corresponding weights $\omega_k^{(e)i}$.

3.6.2 The PDF Representation of Continuous State: Birth Density

If a particle is representing an existing track, the systems dynamics are used as prior information. However, this is not possible for the case of the calculation of the birth density, denoted as $p(x_k \mid E_k = 1, E_{k-1} = 0, Y_k)$, since it is assumed that the signal does not exist at time $k-1$. In this case the birth particles defined as $x_k{}^{(b)i}$ are placed to the state were they could be expected to yield high likelihood. The birth particles are uniformly distributed within the highest intensity bins. It is assumed that even low SNR signals will instantaneously disturb the underlying noise. In this case the data is used to draw samples to form part of the initial state vector $x_k{}^{(b)i}$, the carrier frequency $fc_k{}^{(b)i}$, the energy $A_k{}^{(b)i}$ and the time of arrival $tc_k{}^{(b)i}$. The selection of the PRI is done according to the procedure described in 3.6.4. The algorithm for the calculation of $p(x_k \mid E_k = 1, E_{k-1} = 0, Y_k)$ consists of the following steps.

1. In order to create a set of N_b number of birth particles; the newborn particles are placed uniformly to the $nhigh$ number of highest intensity bins:

$$x_k{}^{(b)i} \sim q(x_k \mid E_k = 1, E_{k-1} = 0, y_k) \quad \forall i \in 1....N_b \qquad \textbf{(3-27)}$$

2. The un-normalized particle weights are calculated using the likelihood ratio given in the Equation (3-14) as [17]:

$$\omega u_k{}^{(b)i} = \frac{L(y_k \mid x_k{}^{(b)i}, E_k)\, p(x_k{}^{(b)i} \mid E_k{}^{(b)i} = 1, E_{k-1}{}^{(b)i} = 0)}{N_b q(x_k{}^{(b)i} \mid E_k{}^{(b)i} = 1, E_{k-1}{}^{(b)i} = 0, y_k)} \qquad \textbf{(3-28)}$$

where $\dfrac{p(x_k{}^{(b)i} \mid E_k{}^{(b)i} = 1, E_{k-1}{}^{(b)i} = 0)}{q(x_k{}^{(b)i} \mid E_k{}^{(b)i} = 1, E_{k-1}{}^{(b)i} = 0, y_k)} = \dfrac{nhigh}{total \;\; number \;\; of \;\; bins}$ given in [17].

3. The weights are normalized as:

$$\omega_k{}^i = \frac{\omega u_k{}^i}{\sum_{n=1}^{N} \omega u_k{}^n} \quad \forall i \in 1....N \qquad \textbf{(3-29)}$$

4. The approximation for the posterior density $p(x_k \mid E_k = 1, E_{k-1} = 0, Y_k)$ is obtained using the set of particles $x_k^{(b)i}$ with corresponding weights $\omega_k^{(b)i}$.

3.6.3 The Probability of Existence

The probability that the signal exist in the data, $P(E_k = 1 \mid Y_k)$, is expanded as [11]:

$$P(E_k = 1 \mid Y_k) = P(E_k = 1, E_{k-1} = 1 \mid Y_k) + P(E_k = 1, E_{k-1} = 0 \mid Y_k) \tag{3-30}$$

By using the definition of conditional probability, each term in the right hand side of this equation can be written as:

$$P(E_k = 1 \mid Y_k) = \frac{p(y_k, E_k = 1, E_{k-1} = 1 \mid Y_{k-1})}{p(y_k \mid Y_{k-1})} + \frac{p(y_k, E_k = 1, E_{k-1} = 0 \mid Y_{k-1})}{p(y_k \mid Y_{k-1})} \tag{3-31}$$

The likelihood values $P(y_k, E_k = 1, E_{k-1} = 1 \mid Y_{k-1})$ and $P(y_k, E_k = 1, E_{k-1} = 0 \mid Y_{k-1})$ are expanded as:

$$\begin{aligned} P(E_k = 1 \mid Y_k) \\ &= \frac{1}{p(y_k \mid Y_{k-1})} \; p(y_k \mid E_k = 1, E_{k-1} = 1, Y_{k-1}) P(E_k = 1, E_{k-1} = 1 \mid Y_{k-1}) \\ &+ \frac{1}{p(y_k \mid Y_{k-1})} \; p(y_k \mid E_k = 1, E_{k-1} = 0, Y_{k-1}) P(E_k = 1, E_{k-1} = 0 \mid Y_{k-1}) \end{aligned} \tag{3-32}$$

The equations $P(E_k = 1, E_{k-1} = 1 \mid Y_{k-1})$ and $P(E_k = 1, E_{k-1} = 0 \mid Y_{k-1})$ can be written in terms of P_b, P_d and the probability of existence at time $k-1$ $P(E_{k-1} = 1 \mid Y_{k-1})$ to give:

$$\begin{aligned} P(E_k = 1 \mid Y_k) \\ &= \frac{1}{p(y_k \mid Y_{k-1})} \; p(y_k \mid E_k = 1, E_{k-1} = 1, Y_{k-1})(1 - P_d) P(E_{k-1} = 1 \mid Y_{k-1}) \\ &+ \frac{1}{p(y_k \mid Y_{k-1})} \; p(y_k \mid E_k = 1, E_{k-1} = 0, Y_{k-1})(P_b)[1 - P(E_{k-1} = 1 \mid Y_{k-1})] \end{aligned} \tag{3-33}$$

If the numerator and denominator of the equation (3-33) are divided by $p(y_k \mid E_k = 0)$ which is the background noise density, then (3-33) becomes a function of the likelihood ratio and can be written as given in Equation (3-34).

$$\begin{aligned} P(E_k = 1 \mid Y_k) \propto\ & L(y_k \mid E_k = 1, E_{k-1} = 1, Y_{k-1})(1 - P_d) P(E_{k-1} = 1 \mid Y_{k-1}) \\ & + L(y_k \mid E_k = 1, E_{k-1} = 0)(P_b)[1 - P(E_{k-1} = 1 \mid Y_{k-1})] \end{aligned} \qquad \textbf{(3-34)}$$

The measurement likelihood ratio $L(y_k \mid E_k = 1, E_{k-1} = 1, Y_{k-1})$ can be found as follows:

$$\begin{aligned} & L(y_k \mid E_k = 1, E_{k-1} = 1, Y_{k-1}) \\ & = \int L(y_k \mid x_k, E_k = 1) p(x_k \mid E_k = 1, E_{k-1} = 1, Y_{k-1}) dx_k \end{aligned} \qquad \textbf{(3-35)}$$

The measurement likelihood ratio $L(y_k \mid E_k = 1, E_{k-1} = 0)$ for birth particles can be found as follows:

$$\begin{aligned} & L(y_k \mid E_k = 1, E_{k-1} = 0) \\ & = \int L(y_k \mid x_k, E_k = 1) p(x_k \mid E_k = 1, E_{k-1} = 0) dx_k \end{aligned} \qquad \textbf{(3-36)}$$

The conditional likelihood $p(y_k \mid Y_{k-1})$ can be expanded by conditioning on E_k and E_{k-1}. With this expansion the term $\dfrac{p(y_k \mid Y_{k-1})}{p(y_k \mid E_k = 0)}$ can be expressed as:

$$\begin{aligned} \frac{p(y_k \mid Y_{k-1})}{p(y_k \mid E_k = 0)} = & L(y_k \mid E_k = 1, E_{k-1} = 1, Y_{k-1})(1 - P_d) P(E_{k-1} = 1 \mid Y_{k-1}) \\ & + L(y_k \mid E_k = 1, E_{k-1} = 0)(P_b)[1 - P(E_{k-1} = 1 \mid Y_{k-1})] \\ & + P_d P(E_{k-1} = 1 \mid Y_{k-1}) + (1 - P_b)[1 - P(E_{k-1} = 1 \mid Y_{k-1})] \end{aligned} \qquad \textbf{(3-37)}$$

Equations (3-34) and (3-37) give the required probability of existence [11].

3.6.4 PRI Modeling

In this work we assume that the value of the PRI is not known however, it has a prior density. A priory density is defined by considering possible PRI values, i.e., PRI is assumed to be around some pre determined specific values and modeled as a mixture of Gaussian around these values. In particular we have selected the means of the mixtures as $0.5 \quad 1 \quad 1.5 \quad 2$ where the unit is in seconds with equal weight and variance 0.01. The PRI value for each particle is drawn from this density denoted as $\beta(x)$:

$$\beta(x) = w_1 N(x\,|\,0.5, 0.01) + w_2 N(x\,|\,1, 0.01) + w_3 N(x\,|\,1.5, 0.01) + w_4 N(x\,|\,2, 0.01) \qquad \textbf{(3-38)}$$

where the $w_1 \quad w_2 \quad w_3 \quad w_4$ are the mixture weights and they equal to $w_i = 0.25$ for $\forall i \in \ 1...4\ $.

The plot of a priory distribution of PRI, $\beta(x)$, is given in Figure 3.3.

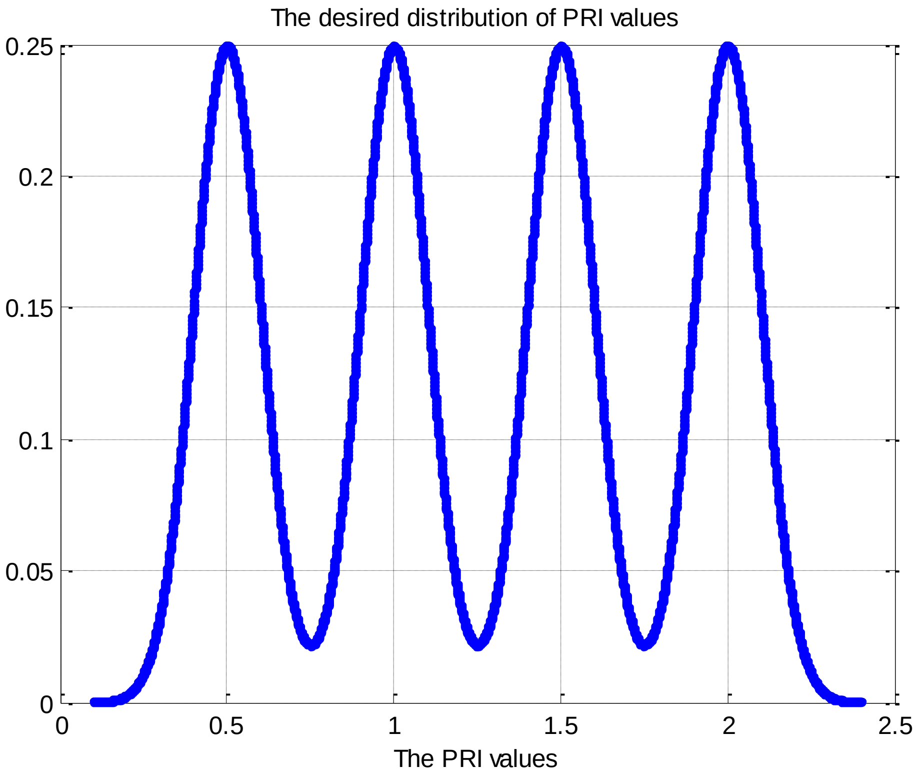

Figure 3.3 A priory distribution for the PRI values of the particles

Metropolis-Hastings algorithm described in 2.2.1 is used to draw samples from this distribution. The candidate-generating density is a 1D Gaussian $q(x' \mid x) = N(x' \mid x, \sigma_p)$, where σ_p is a parameter of the proposal.

The histogram of the samples which will be used to assign the PRI values of particles are given in Figure 3.4 . The variance of the candidate-generating density is chosen as $\sigma_p^2 = 5^2$ and the number of samples is $N = 1000$.

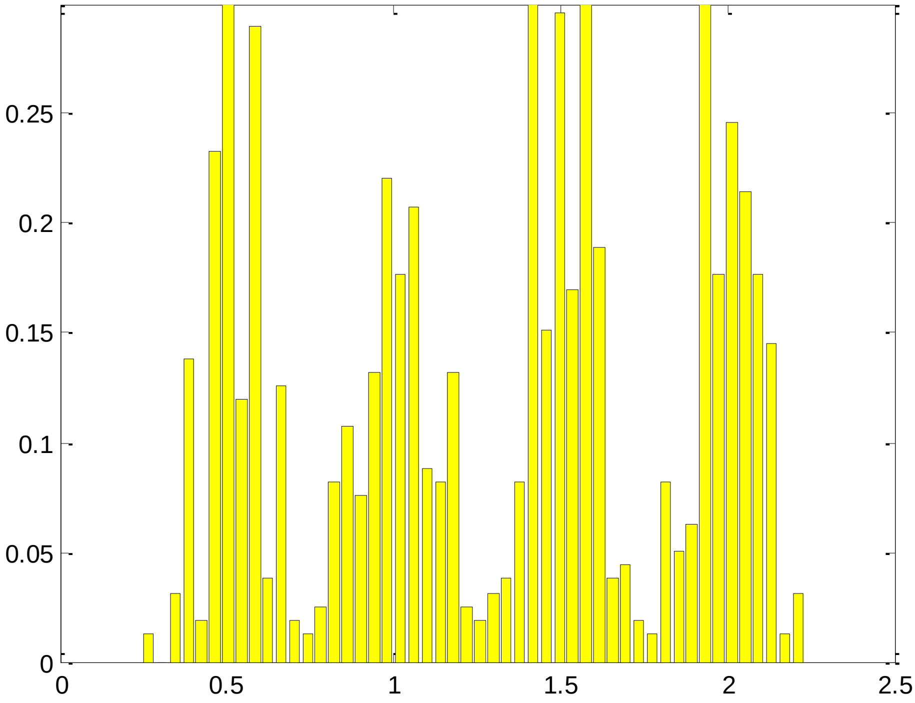

Figure 3.4 The histogram of the samples obtained for PRI value

3.6.5 The Complete Algorithm

$x_k = \quad fc_k \quad PRI_k \quad A_k \quad tc_k \quad ^T$ is the continuous state of our model and it must be initiated at time $k = 1$ by finding N vectors which correspond to part of N initial particles. Initial fc_k, A_k and tc_k values are drawn from the highest intensity bins since they are necessarily birth particles at time $k=1$. Initial PRI is drawn from the Gaussian mixture density explained in the previous section.

In the problem, as it is stated earlier the signal's duty percent is quite low. To get the measurement spectrogram of the signal is computed with a certain frame rate. Consecutive frames of certain number are considered as a 'measurement frame'. For example, for the data shown in Figure 3.6 measurement frame's length is selected as $0.5\sec$. Figure 3.5 shows the spectrogram of in the signal under noise for 10 seconds, so in this figure there are 20 measurement frames. In other words, the data for $time = 0:0.5\sec$ will form the first measurement frame and the data for $time = 0.5:1\sec$ will be considered as $2nd$ measurement frame, etc. It can be observed that there is a signal circled in red in the $2nd$ and $5th$ measurement frames, but there are no pulses in $3rd$ and $4th$ frames. The existing particles are updated if there is an expected pulse on that frame according to PRI value. In other words, not all of the existing particles are updated in each frame; updating is done if and only if the time of arrival parameter of the pulse for that particle is in the limits of the concerning frame, then the existing particle is updated using the procedure described in 3.6.1.

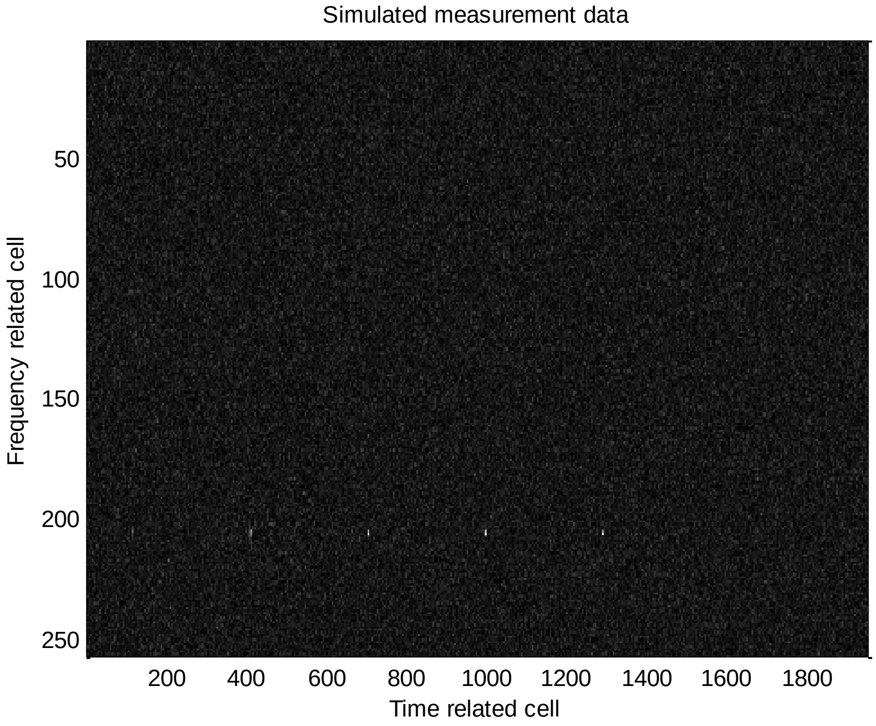

Figure 3.5 The simulated data with peak SNR 19.3 dB, the carrier frequency $fc = 20kHz$, the PRI $PRI = 1.5\sec$ and the pulse width $PW = 20\text{msec}$

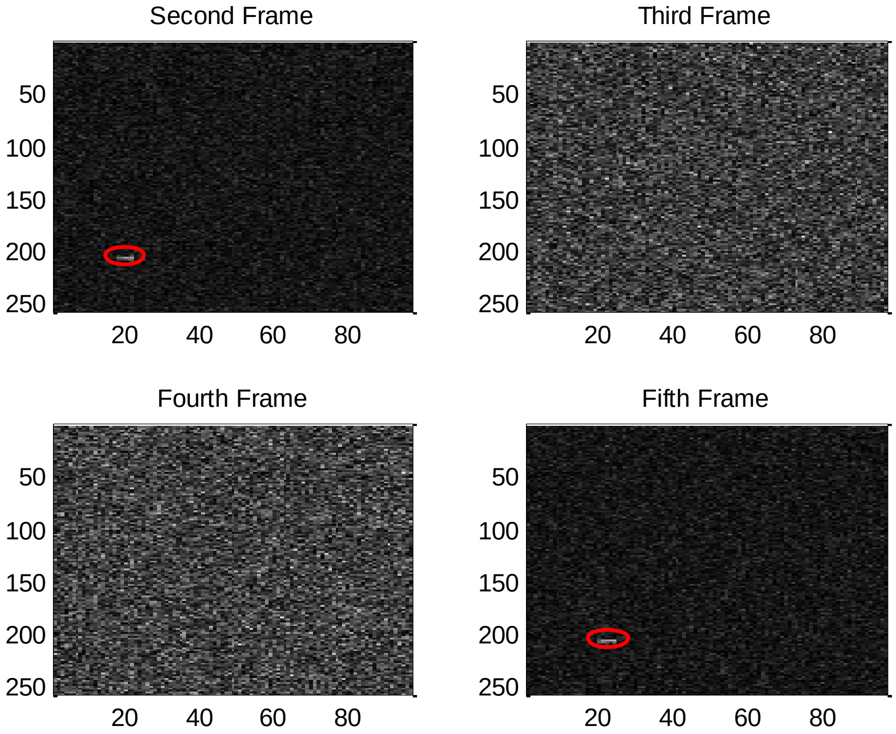

Figure 3.6 The measurement frames, each corresponds to data of $0.5\sec$

After updating of the existing particles, the number of efficient particles is computed. If the number of efficient particles is lower than the predetermined threshold (if $N_{eff} < N_{thr}$) then re-sampling is done. The purpose of re-sampling step is to eliminate the samples with low importance weights and replicate the samples with high importance weights.

The next step is to estimate the signal state. The carrier frequency and the time of arrival of the pulses are estimated using the minimum mean-square error (MMSE) estimation given in Equation (3-39).

$$E\ x_k\ = \sum_{i=1}^{N} \omega_k{}^i x_k{}^i \qquad \textbf{(3-39)}$$

The following step is the so called death-birth process where some of the particles are declared as dead randomly by applying the Markov transition matrix given in (3-4). It is desired to have the number of particles constant, therefore new particles are born after the death process. In other words, the number of birth particles is equal to the number of death particles. By using the procedure explained in 3.6.2, the birth particles are assigned.

The final step is to calculate the probability of existence. In order to calculate $P(E_k = 1 | Y_k)$, the terms $L(y_k | E_k = 1, E_{k-1} = 1, Y_{k-1})$ and $L(y_k | E_k = 1, E_{k-1} = 0)$ should be computed as shown in equation (3-34). Using the existence particles these terms can be approximated by $L(y_k | E_k = 1, E_{k-1} = 1, Y_{k-1}) \approx \sum_{i=1}^{N_e} \omega u_k{}^{(e)i}$ and $L(y_k | E_k = 1, E_{k-1} = 0) \approx \sum_{i=1}^{N_b} \omega u_k{}^{(b)i}$ where $\omega u_k{}^{(e)i}$ and $\omega u_k{}^{(b)i}$ denote the un-normalized existing particles and the un-normalized birth particles respectively [11]. Finally, the probability of existence at frame k is computed.

$$\begin{aligned}
&\mathrm{A} = \sum_{i=1}^{N_e} \varpi u_k{}^{(e)i} (1-P_d) P(E_{k-1}=1 \mid Y_{k-1}) \\
&B = \sum_{i=1}^{N_b} \varpi u_k{}^{(b)i} (P_b)[1-P(E_{k-1}=1 \mid Y_{k-1})] \\
&P(E_k=1 \mid Y_k) \approx \frac{\mathrm{A}+\mathrm{B}}{\mathrm{A}+\mathrm{B}+(P_d)P(E_{k-1}=1 \mid Y_{k-1})+(1-P_b)[1-P(E_{k-1}=1 \mid Y_{k-1})]}
\end{aligned} \qquad \textbf{(3-40)}$$

Table 3.1 gives a summary of the algorithm.

Table 3.1 Particle Filter for Track-Before-Detect Algorithm

```
Given the observed data $y_k$ at measurement frame $k$ assuming that $N$ particles
with $x_{k-1}^i, \omega_{k-1}^i$ is available , do
• FOR $i = 1:N$
    o IF time of the pulse arrival for the particle $x_{k-1}^i$ is at that frame $k$ then,
        ▪ Draw $x_k^i \sim q(x_k \mid x_{k-1}^i, E_k = 1, E_{k-1} = 1, y_k)$
        ▪ Calculate the un-normalized weights using $\omega u_k^i = \frac{1}{N_e} L(y_k \mid x_k^i, E_k)$
      (The Existing Particles procedure explained in 3.6.1 )
    o ELSE
        ▪ Assign $x_k^i = x_{k-1}^i \;\forall i \in 1....N$ (To preserve the state of the particles which is not updated for this frame)
        ▪ Assign $\omega u_k^i = \omega_{k-1}^i \;\forall i \in 1....N$ (To preserve the weights of the particles which is not updated for this frame)
• End FOR
• Normalize the weights: $\omega_k^i = \frac{\omega u_k^i}{\sum_{n=1}^{N} \omega u_k^n} \;\forall i \in 1....N$
• Calculate $N_{eff} = \frac{1}{\sum_{i=1}^{N} (\omega_k^i)^2}$
• IF $N_{eff} < N_{thr}$
    o Resample $x_k^i, \omega_k^i$ to obtain the new set of particles resampled set.
• END IF
```

Table 3.1 continued

- Estimate the signal state using $E \;\; x_k \;\; = \sum_{i=1}^{N} \omega_k{}^i x_k{}^i$
- Apply Markov Chain $E_k = \Pi E_{k-1}$ where $\Pi = \begin{bmatrix} 1-P_b & P_b \\ P_d & 1-P_d \end{bmatrix}$ to kill the particles randomly, the number of particles that are dead denoted as N_b .
- FOR $i = 1 : N_b$
    - Draw $x_k{}^{(b)i} \sim q(x_k \mid E_k = 1, E_{k-1} = 0, y_k)$
    - Calculate the un-normalized weights using $$\omega u_k{}^i = \frac{L(y_k \mid x_k{}^{(b)i}, E_k)\, p(x_k{}^{(b)i} \mid E_k{}^{(b)i} = 1, E_{k-1}{}^{(b)i} = 0)}{N_b q(x_k{}^{(b)i} \mid E_k{}^{(b)i} = 1, E_{k-1}{}^{(b)i} = 0, y_k)}$$

    (The Birth Particles procedure explained in 3.6.2)
- End FOR
- Normalize the weights: $\omega_k{}^i = \dfrac{\omega u_k{}^i}{\sum_{n=1}^{N} \omega u_k{}^n} \quad \forall i \in \; 1....N$
- Calculate the probability of existence using the equations
- $$\mathrm{A} = \sum_{i=1}^{N_e} \omega u_k{}^{(e)i} (1-P_d) P(E_{k-1} = 1 \mid Y_{k-1})$$ $$B = \sum_{i=1}^{N_b} \omega u_k{}^{(b)i} (P_b)[1 - P(E_{k-1} = 1 \mid Y_{k-1})]$$ $$P(E_k = 1 \mid Y_k) \approx \frac{\mathrm{A} + \mathrm{B}}{\mathrm{A} + \mathrm{B} + (P_d) P(E_{k-1} = 1 \mid Y_{k-1}) + (1-P_b)[1 - P(E_{k-1} = 1 \mid Y_{k-1})]}$$

where $\omega u_k{}^{(e)i}$ and $\omega u_k{}^{(b)i}$ denote the unnormalized existing particles and the unnormalized birth particles respectively.

3.7 *Simulations*

We have implemented our algorithm for a specific simulated problem that can be considered somewhat realistic. In this part these simulations are presented.

In the first simulation, the signal has amplitude of 0.01 and the pulse width of $PW = 20\text{msec}$, the pulse repetition rate is $PRI = 1.5\sec$ and the carrier frequency is $fc = 20kHz$. The peak SNR is 9.79 dB and the average SNR is -8.96 dB. The signal in time domain is shown in Figure 3.7. The spectrogram of the signal is computed and a Gaussian noise with the variance $\sigma_w{}^2 = 0.1$ is added to each bin. The data generated in this way is divided into frames in time corresponding to $0.5\sec$, so if the total simulation time is $10\sec$, there will be 20 frames. In the simulated data, there are five pulses at the measurement frames $k = 2, k = 5, k = 8, k = 11 \;\; and \;\; k = 14$. All the other frames contain only noise in the data. In the time domain, the pulses appear at $time = 0.6, time = 2.1, time = 3.6, time = 5.1 \;\; and \;\; time = 6.6$.

The whole simulated data is shown in Figure 3.8 and the $2nd$, $3rd$, $4th$ and $5th$ measurement frames are given in Figure 3.9. There is signal circled in red in the $2nd$ and $5th$ frames, but there is no pulse in $3rd$ and $4th$ frames.

The number of particles is $N = 1000$ and the resampling is done if the efficient number of particles N_{eff} is below the number of particle threshold $N_{thr} = N/3$ (if $N_{eff} < N_{thr}$).

The parameters in the Markov Chain is chosen such that the probability of birth $P_b = 0.2$ and the probability of death $P_d = 0.2$. The sampling frequency is chosen as $fs = 50kHz$ and 512 point FFT is used. The initial probability of existence is 0.05.

As its is stated, the state vector is represented as $x_k = \begin{bmatrix} fc_k & PRI_k & A_k & tc_k \end{bmatrix}^T$ where x_k consists of the carrier frequency fc_k, the PRI PRI_k, the power A_k and the time of the arrival of the pulse tc_k. The birth particles are uniformly distributed within the 100 highest intensity bins. Therefore the carrier frequency fc_k, the power A_k and the time of arrival of the pulse tc_k are attained from the data. The PRI of the particles are assigned using the procedure described in 3.6.4.

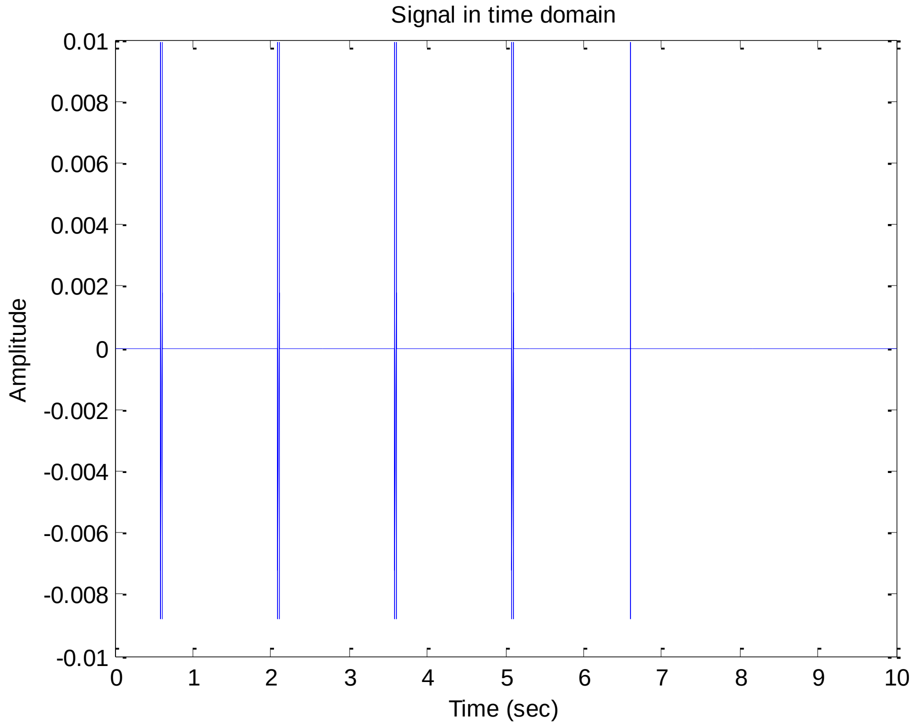

Figure 3.7 The signal in time domain, the amplitude is $amp = 0.01$, the carrier frequency $fc = 20kHz$, the PRI $PRI = 1.5\sec$ and the pulse width $PW = 20\text{msec}$

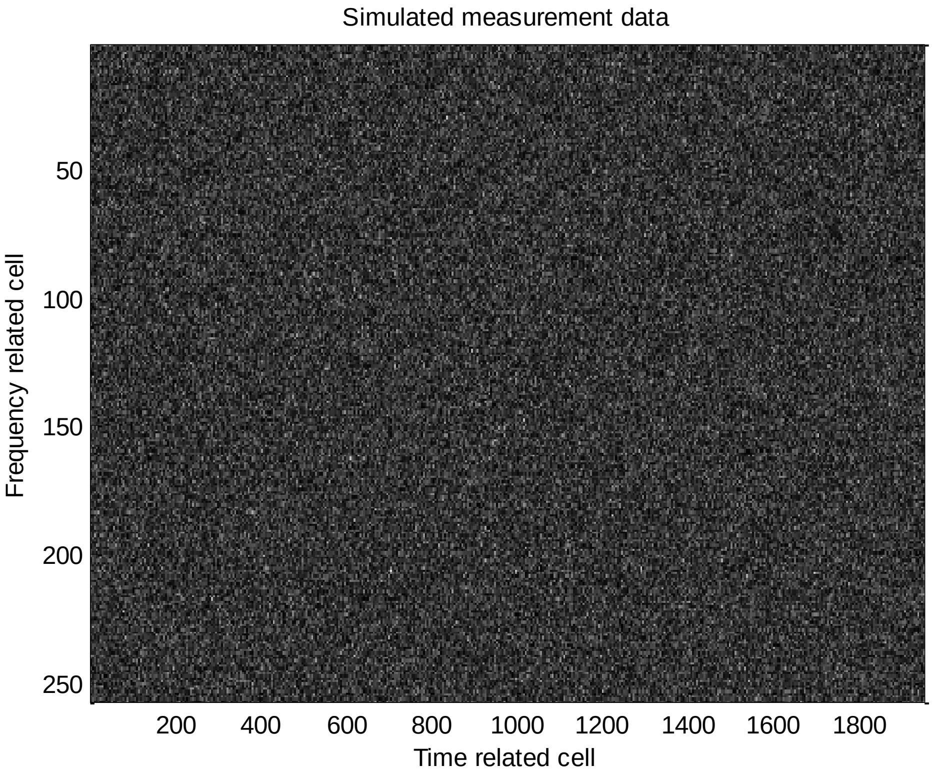

Figure 3.8 The entire spectrogram in noise

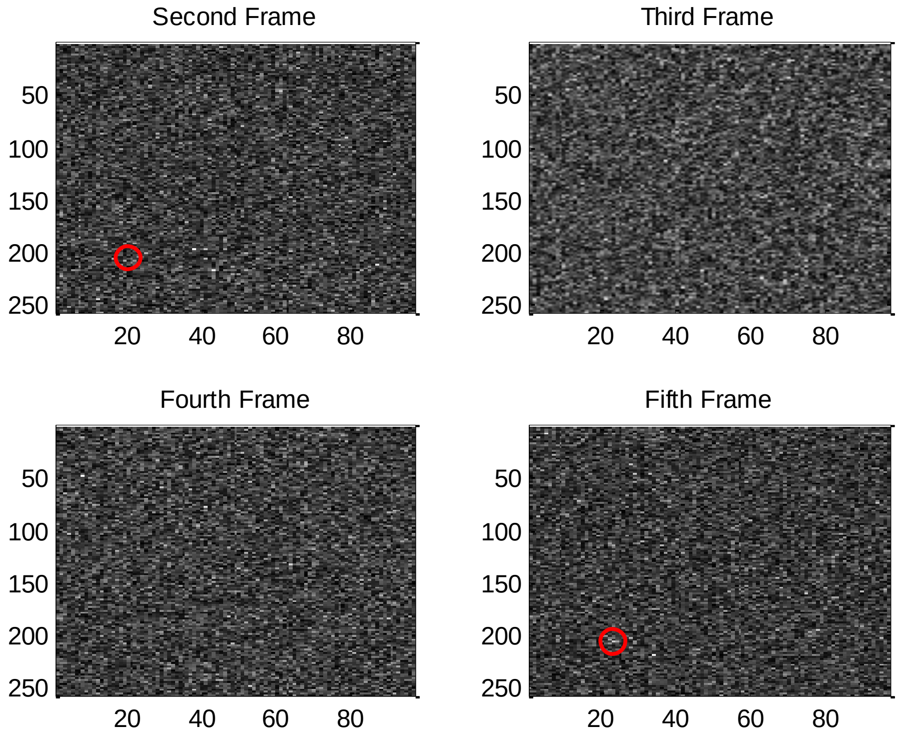

Figure 3.9 The measurement frames of $2nd$**,** $3rd$**,**$4th$ **and** $5th$

The results consists the following plots:

- The histogram of the carrier frequency of the particles at frames 2, 5, 7, 11, and 17
- The plot of the carrier frequency component vs. the weights of the particles
- The estimated carrier frequency vs. frame
- The arrival time of the pulses vs. frame
- The probability of existence vs. frame

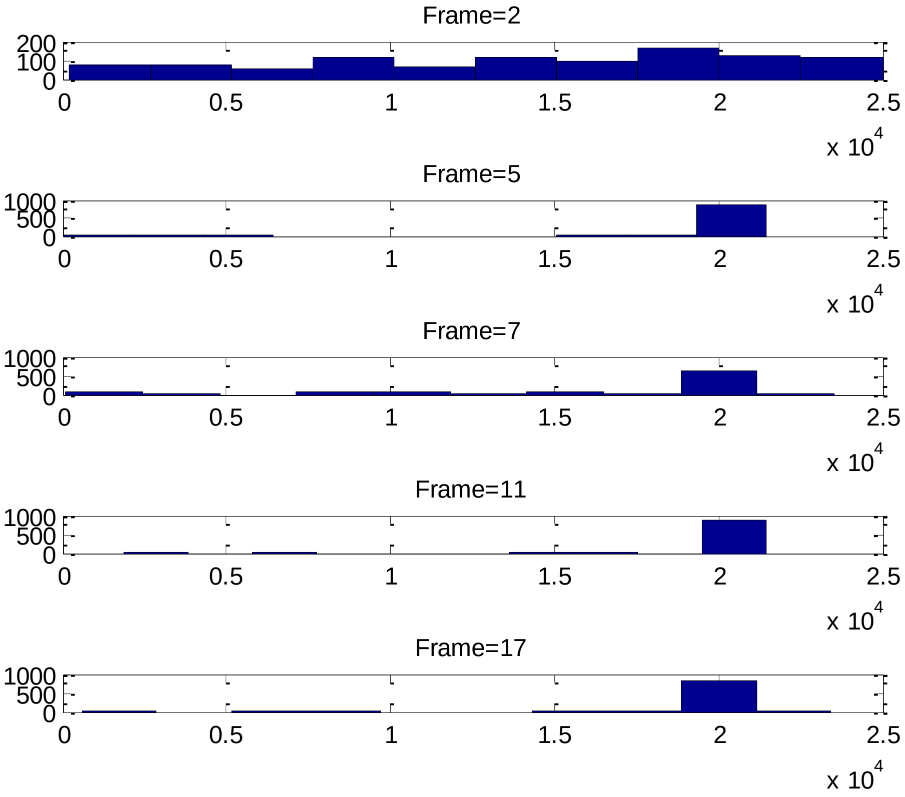

Figure 3.10 The histogram of the carrier frequency of the particles

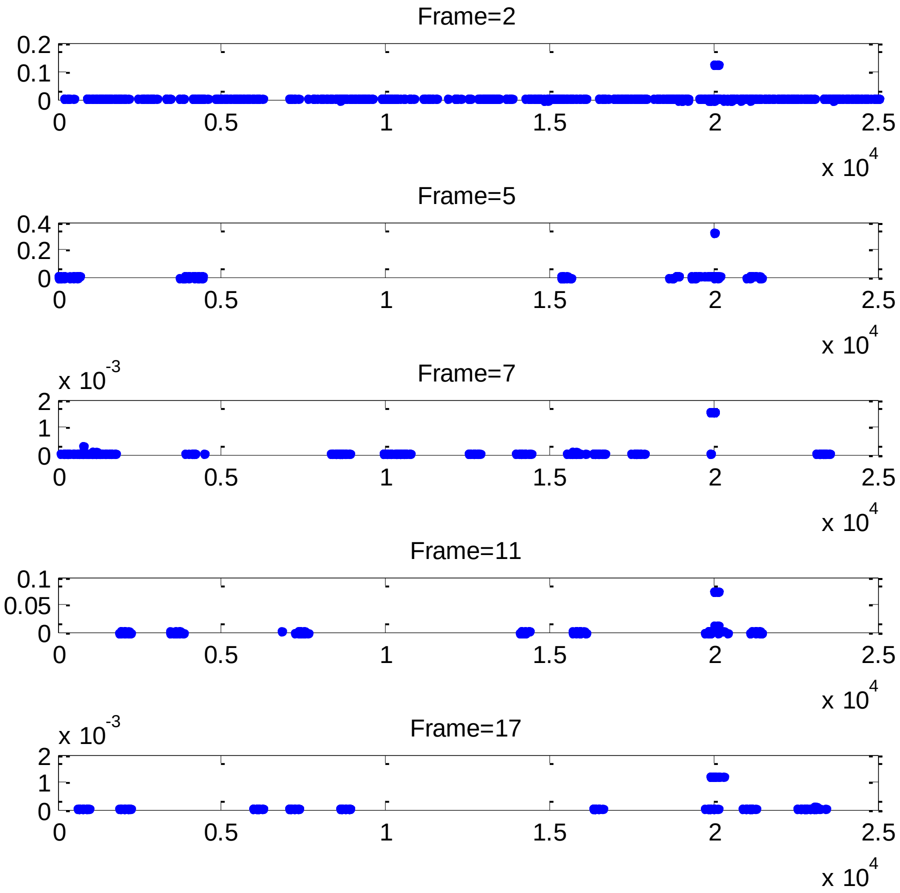

Figure 3.11 The carrier frequency component vs. the weights of the particles

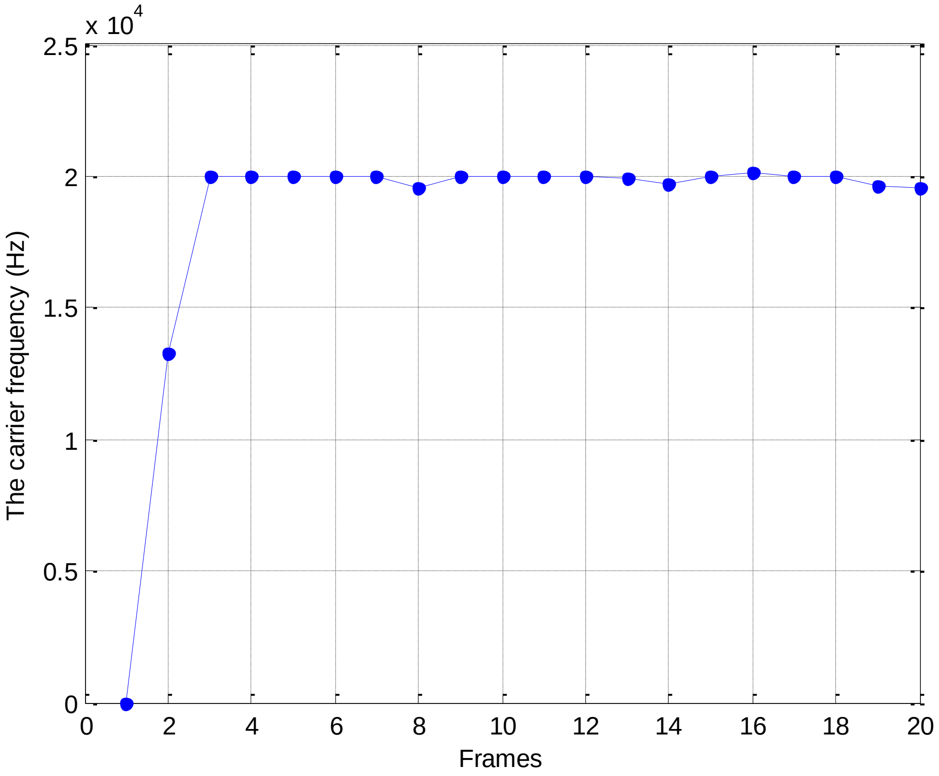

Figure 3.12 The estimated carrier frequency vs. frame

The estimated arrival times of the pulses are given below in Figure 3.13. The PRI of the data can be deduced as $PRI = 1.5$ by using the time difference between two consecutive arrival times.

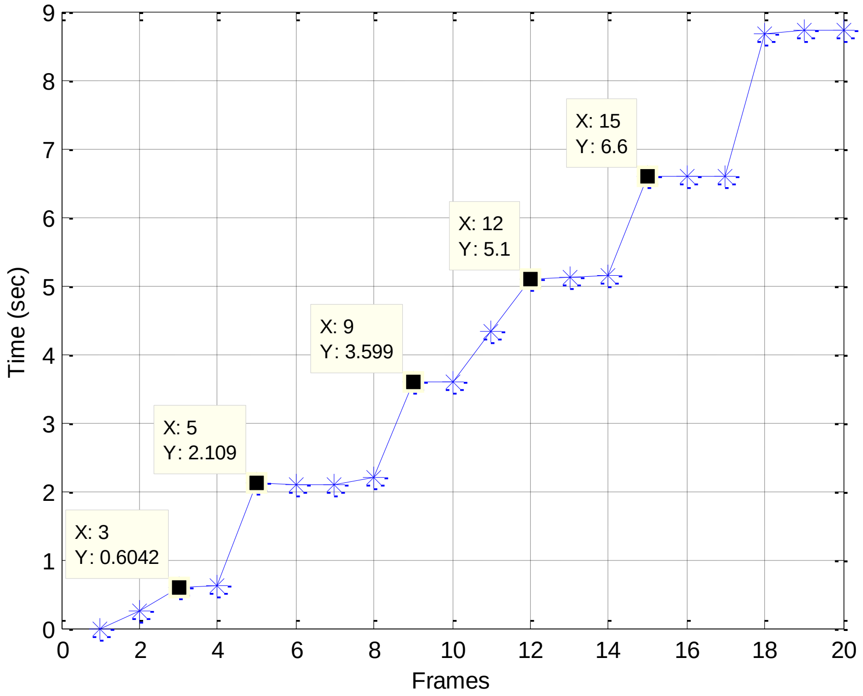

Figure 3.13 The arrival time of the pulses

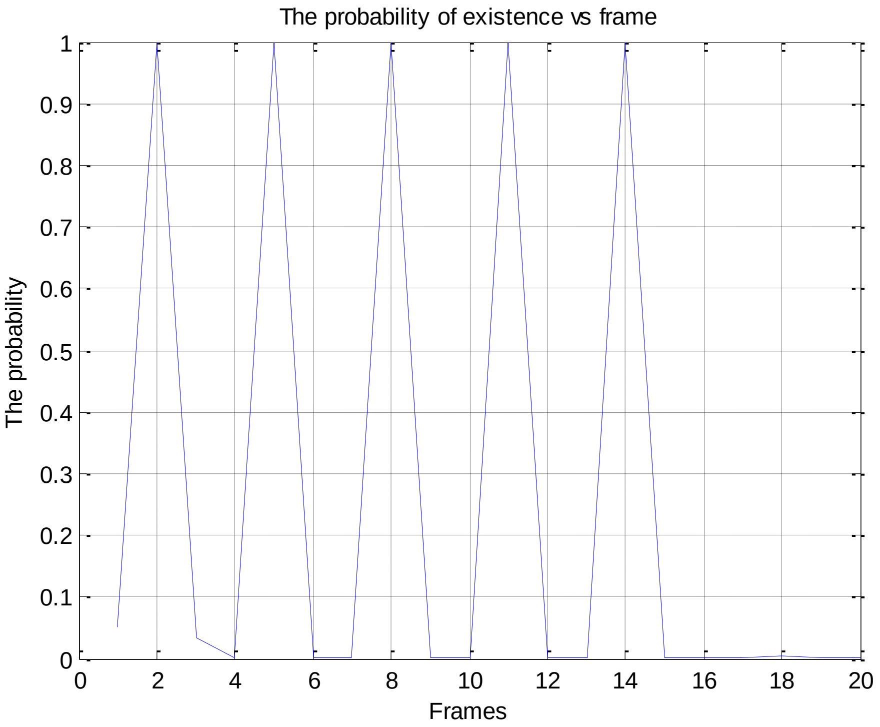

Figure 3.14 The probability of existence vs. frame

In the second simulation, the parameters are the same as with the first simulation except the signal amplitude. The signal has an amplitude of $amp = 0.008$ and the pulse width $PW = 20\text{msec}$, the pulse repetition rate $PRI = 1.5\sec$ and the carrier frequency $fc = 20kHz$. The peak SNR is 7.85 dB and the average SNR is -10.90 dB. The spectrogram of the signal is taken and the Gaussian noise with the variance $\sigma_w^{\,2} = 0.1$ is added to each bin. The pulses appear at $time = 0.6, time = 2.1, time = 3.6, time = 5.1$ *and* $time = 6.6$. The whole simulated data is shown in Figure 3.16 and $2nd$, $3rd$, $4th$ and $5th$ measurement frames are given in Figure 3.17. The signal is circled in red in the $2nd$ and $5th$ frames, but there is no pulse in $3rd$ and $4th$ frames. Since the signal has lower SNR than the first simulation, some of the pulse arrivals cannot be detected. The performance of the carrier frequency and PRI estimation is better in the first simulation compared to this simulation. The plots of the simulated data are given below:

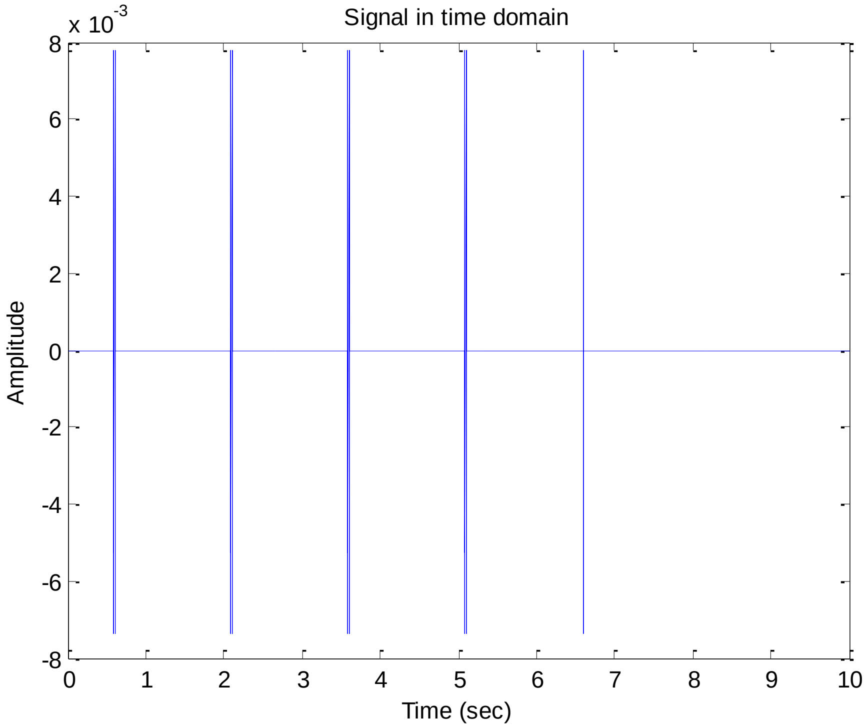

Figure 3.15 The signal in time domain, the amplitude is $amp = 0.008$, the carrier frequency $fc = 20kHz$, the PRI $PRI = 1.5\sec$ and the pulse width $PW = 20\text{msec}$

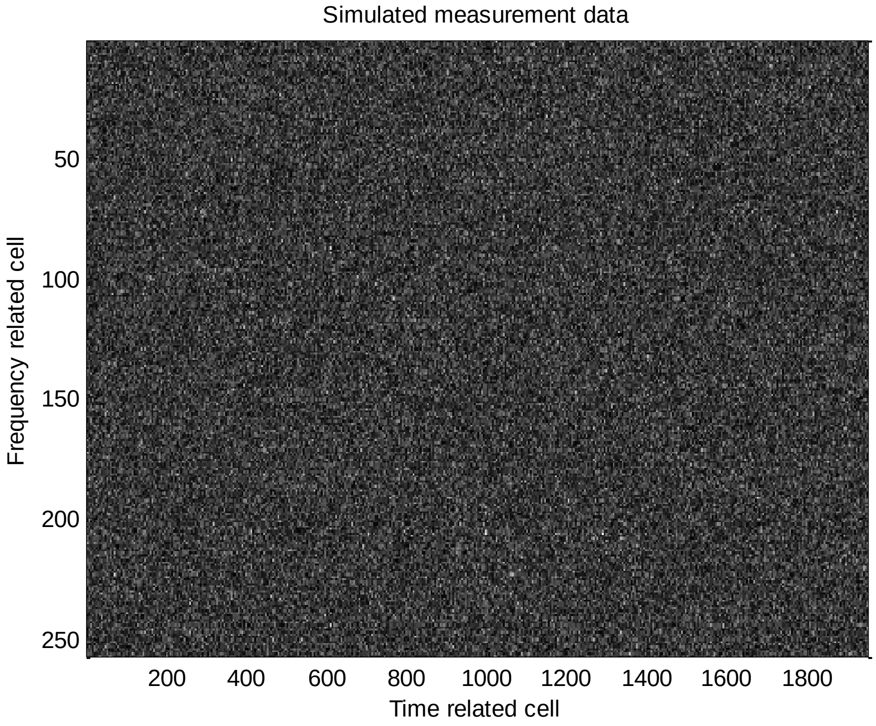

Figure 3.16 The entire spectrogram in noise

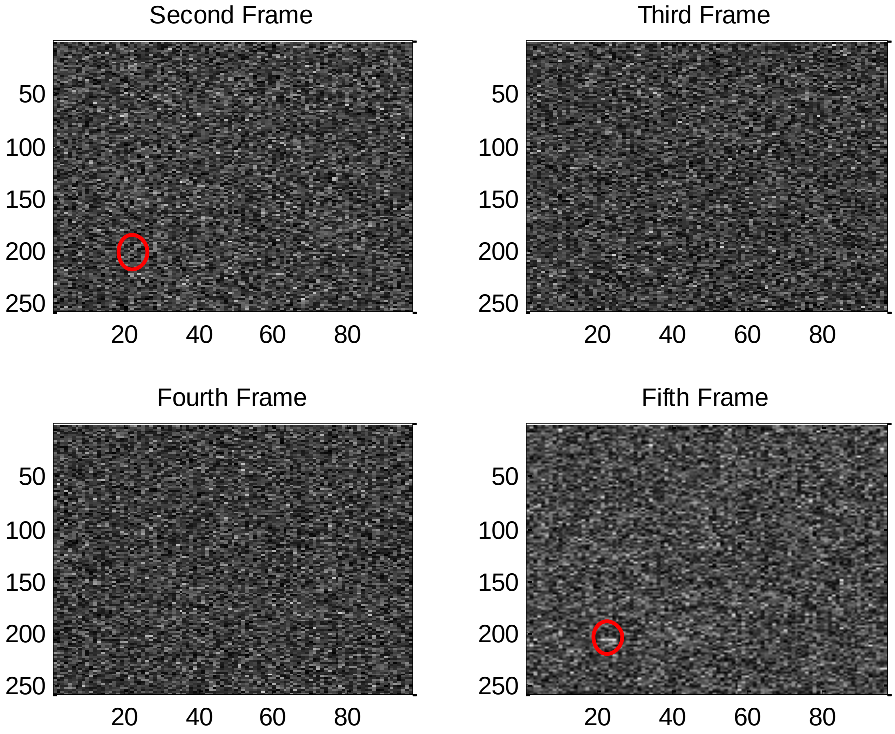

Figure 3.17 The measurement frames of $2nd$**,** $3rd$**,** $4th$ **and** $5th$

The results consists the following plots:

- The histogram of the carrier frequency of the particles at frames 2, 5, 7, 11, and 17
- The plot of the carrier frequency component vs. the weights of the particles
- The estimated carrier frequency vs. frame
- The arrival time of the pulses vs. frame
- The probability of existence vs. frame

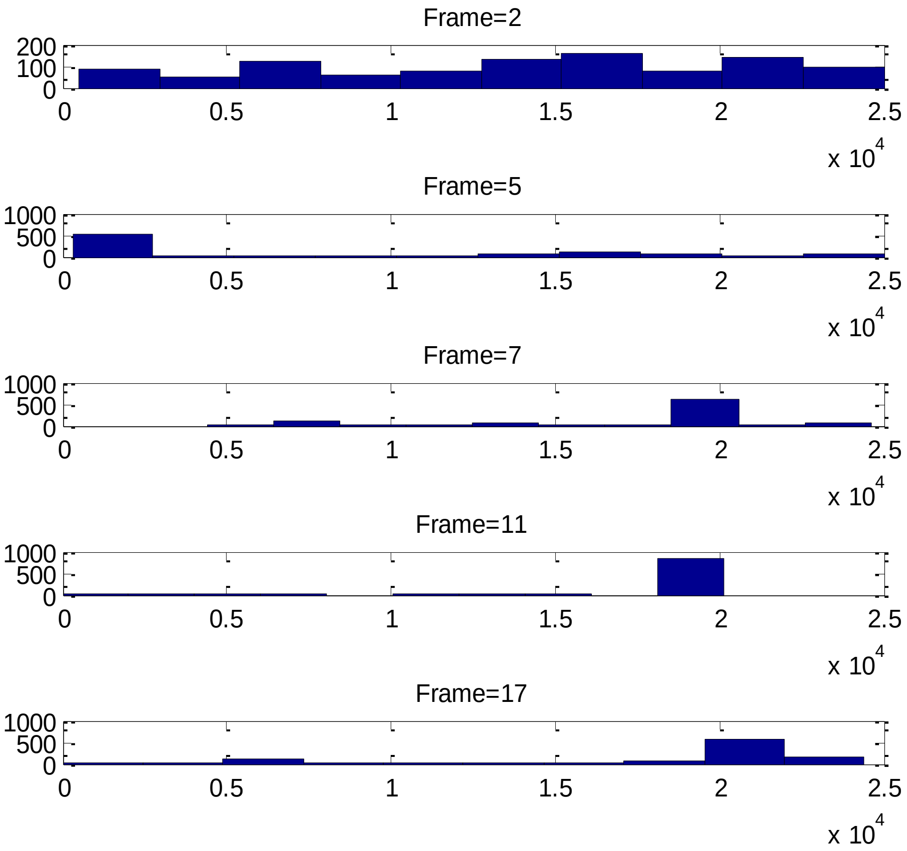

Figure 3.18 The histogram of the carrier frequency of the particles

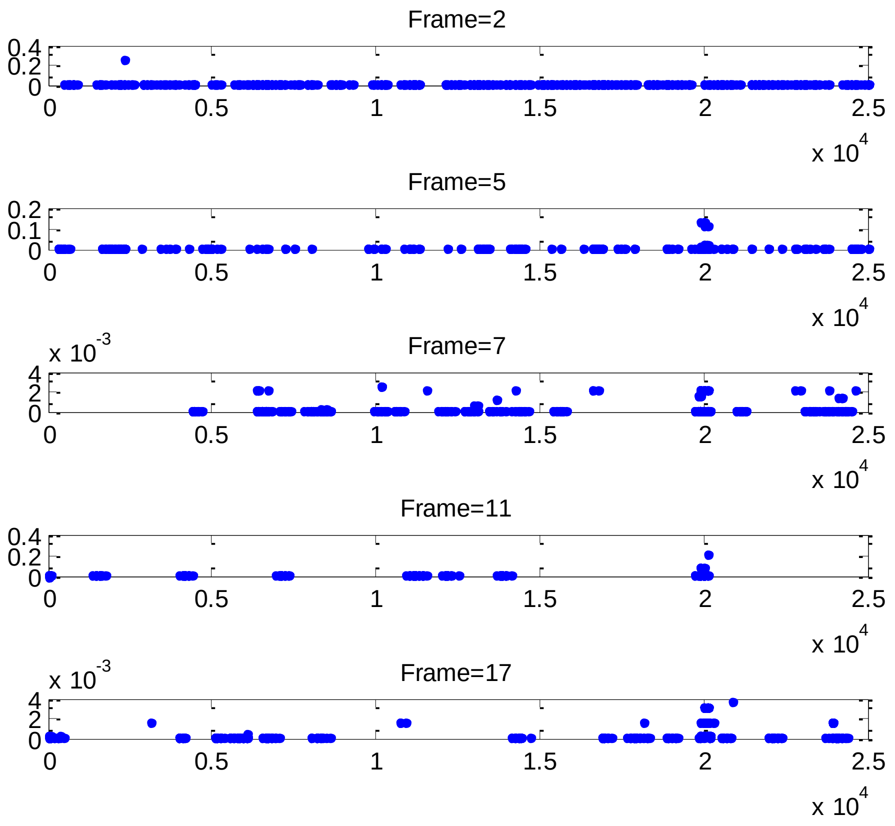

Figure 3.19 The carrier frequency component vs. the weights of the particles

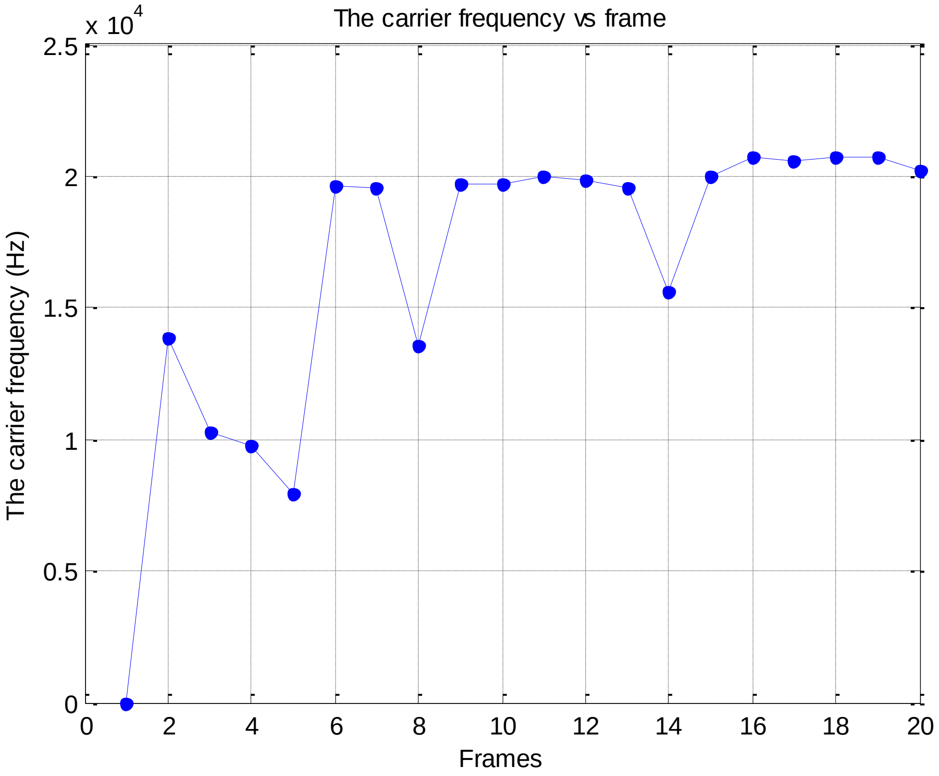

Figure 3.20 The estimated carrier frequency vs. frame

The arrival time of the pulses obtained form the filter is given below in. The PRI of the data can be deduced as $PRI = 1.5$ by using the time difference between two consecutive arrival times.

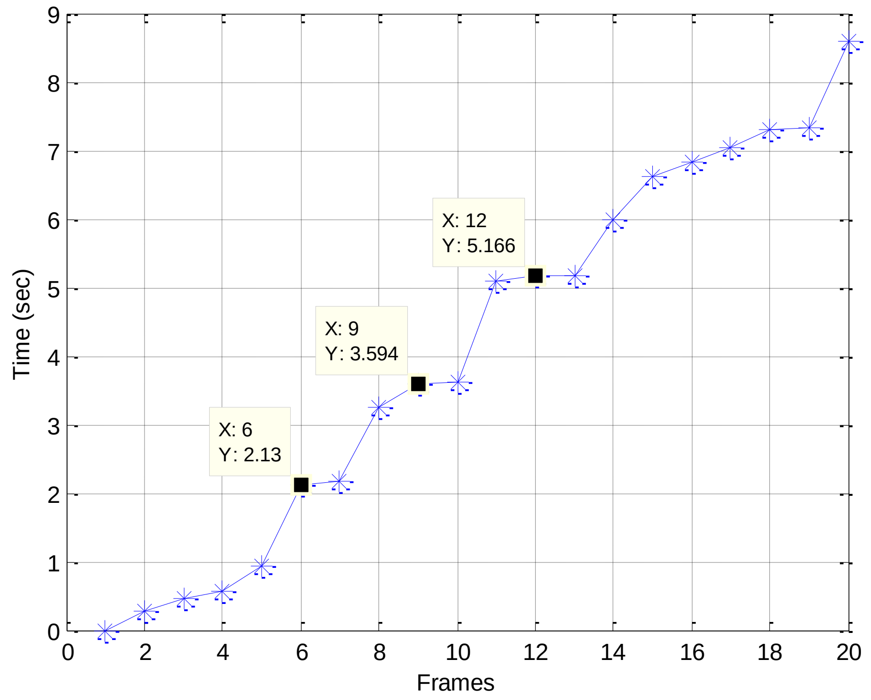

Figure 3.21 The arrival time of the pulses

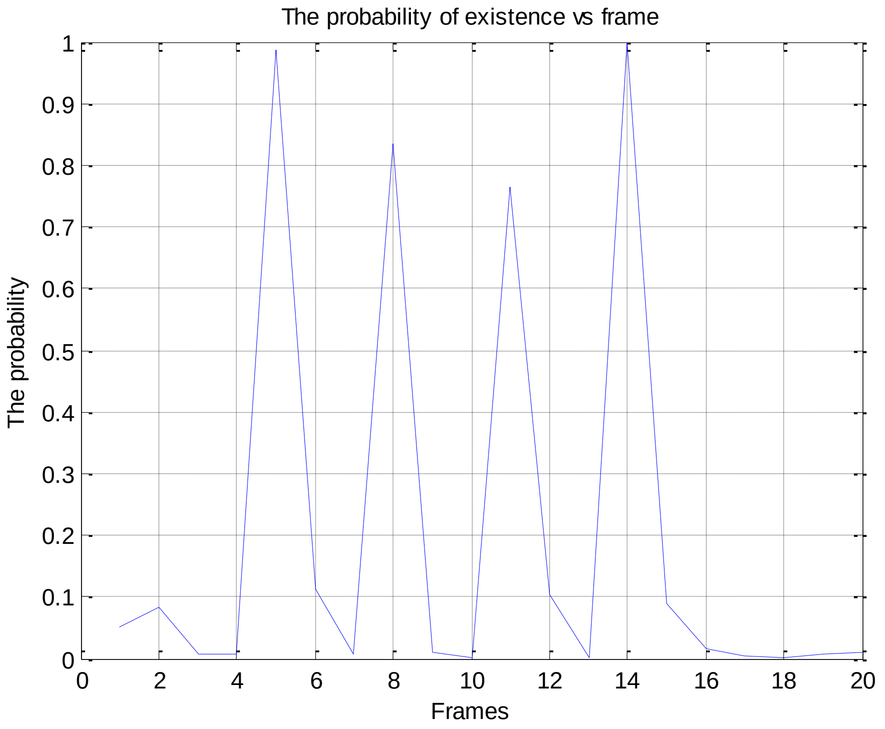

Figure 3.22 The probability of existence vs. frame

In the third simulation, the aim is to get the PRI of the data. The signal has an amplitude of 0.01 and the pulse width $PW = 20\text{msec}$, the pulse repetition rate $PRI = 1\sec$ and the carrier frequency $fc = 20kHz$. The spectrogram of the signal is taken and the Gaussian noise with the variance $\sigma_w{}^2 = 0.1$ is added to each bin. The pulses appear at $time = 0.6, time = 1.6, time = 2.6, time = 3.6$ and $time = 4.6$. In Figure 3.25, 4 consecutive measurement frames are given. There is signal in the 8th and 10th frames circled in red and there is only noise in the others. It is obvious that detecting the existence and the parameters of the signal visually is not possible.

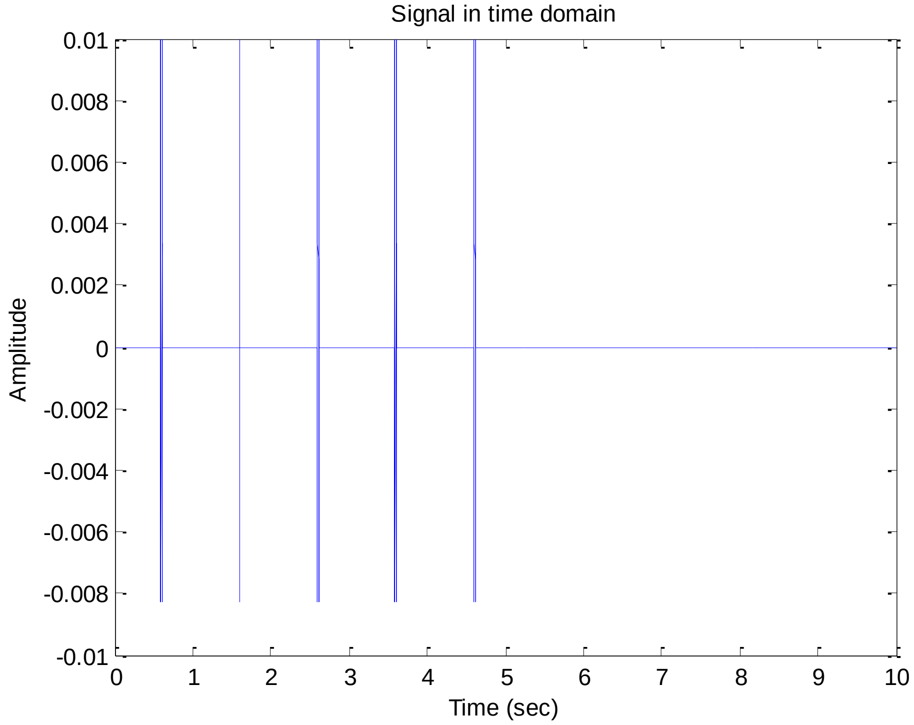

Figure 3.23 The signal in time domain, the amplitude is $amp = 0.01$, the carrier frequency $fc = 20kHz$, the PRI $PRI = 1\sec$ and the pulse width $PW = 20\text{msec}$

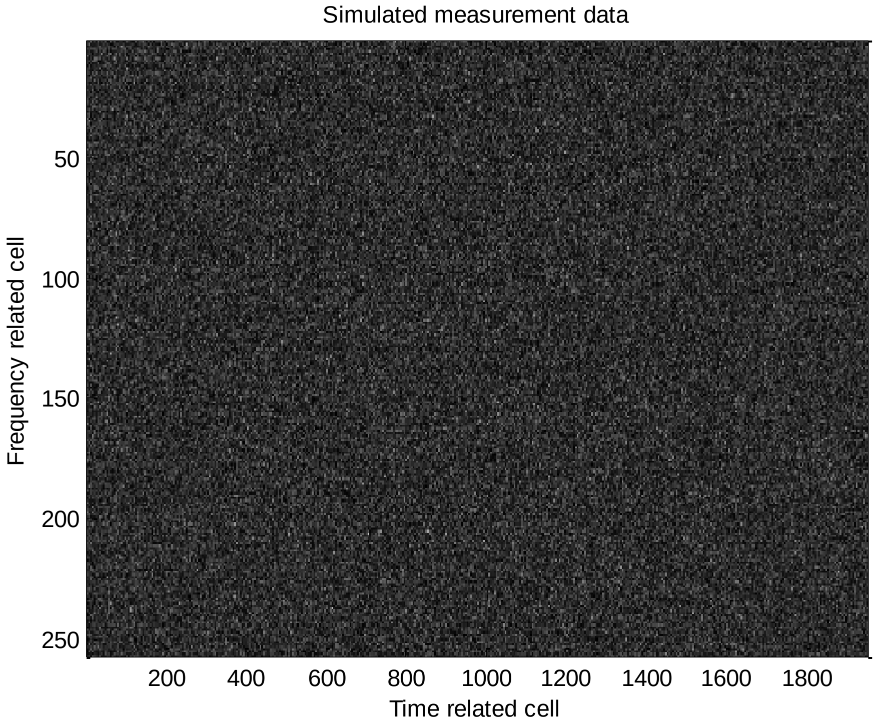

Figure 3.24 The entire spectrogram in noise

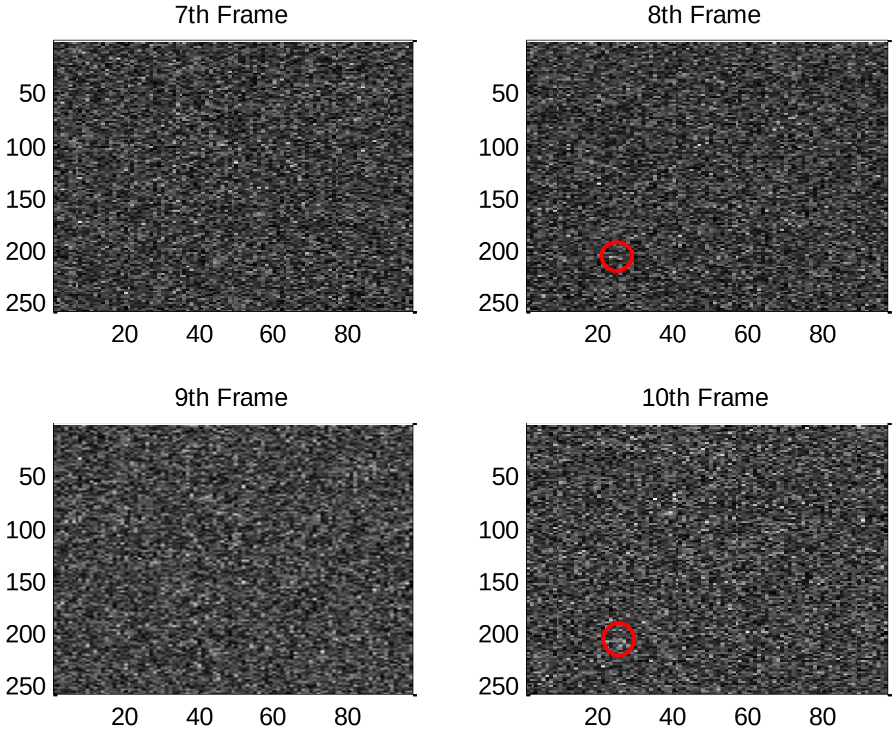

Figure 3.25 The measurement frames of $7th$**,** $8th$**,**$9th$ **and** $10th$

The arrival time of the pulses obtained form the filter is given below in Figure 3.26. The PRI of the data can be deduced as $PRI = 1\text{sec}$ by using the time difference between two consecutive arrival times.

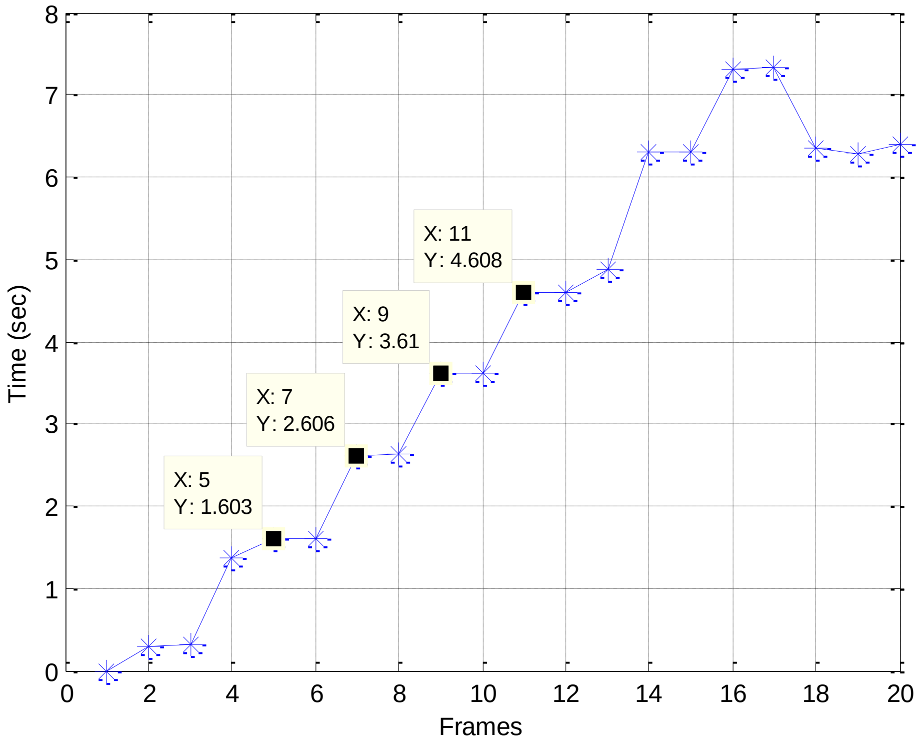

Figure 3.26 The arrival time of the pulses

3.8 *The Performance of the Algorithm*

In this part, the performance of the filter is gauged on average over 50 Monte Carlo runs. The performance of the proposed algorithm is evaluated in terms of root mean square (RMS) errors in carrier frequency. The carrier frequency RMS error is calculated as given in equation (3-41):

$$RMSE(fc) = \sqrt{\frac{1}{MC}\sum_{i=1}^{MC}\ (f_c)_k - (f_{c\_est})_k{}^{2}} \qquad \textbf{(3-41)}$$

where $(f_c)_k$ is the true carrier frequency at frame k, $(f_{c\_est})_k$ is the estimated carrier frequency at frame k, MC is the number of Monte Carlo runs.

Besides the RMS errors in carrier frequency, the results contain average estimated carrier frequency and average probability of existence over 50 runs.

In the following part the Monte Carlo simulation parameters and the plots of the results are given.

3.8.1 Monte Carlo Simulations

The common parameters of the first Monte Carlo Simulations are given in Table 3.2. The amplitude of the signal is changed in two sets. The signal amplitude is 0.01 (peak SNR 9.79 dB) for the first set and the amplitude is 0.008 (peak SNR 7.85 dB) for the second set. 50 Monte Carlo runs are done for each set. The plots of the results are given in Figure 3.27, Figure 3.28 and Figure 3.29.

The average estimated carrier frequency and the RMS error of frequency in the frames where the signal exist are given in Figure 3.27 and Figure 3.28 respectively. These figures show that consistent estimates of the carrier frequency are calculated by the filter. However, the higher amplitude of the signal provides better estimated frequency and lower RMS errors.

The detection performance of the algorithm is shown in terms of the probability of existence in Figure 3.29. This figure demonstrates that the algorithm presented in this thesis can detect signals which cannot be detected by conventional methods. The frames containing pulses have high probability of existence whereas the other frames which do not contain a pulse have probability of existence values lower than 0.1.

Table 3.2 Monte Carlo Simulation Parameters (A)

The carrier frequency, f_c	$15kHz$
The pulse repetition interval, PRI	$1.5\sec$
The pulse width, PW	$20m\sec$
The variance of Gaussian Noise, $\sigma_w{}^2$	0.1
Peak SNR	9.79 dB , for signal amplitude=0.01 7.85 dB , for signal amplitude=0.008
Average SNR	-8.96 dB , for signal amplitude=0.01 -10.90 dB , for signal amplitude=0.008
Total Simulation Time	$10\sec$
Number of Frames (Data is divided into frames in time corresponding to $0.5\sec$)	20
Number Of Pulses in the Data	5 pulses at frame 2,5,8,11 and 14
The sampling frequency, f_s	$50kHz$
The initial probability of existence	0.05
The probability of birth, P_b	0.2
The probability of death, P_d	0.2
Number Of Particles	1000

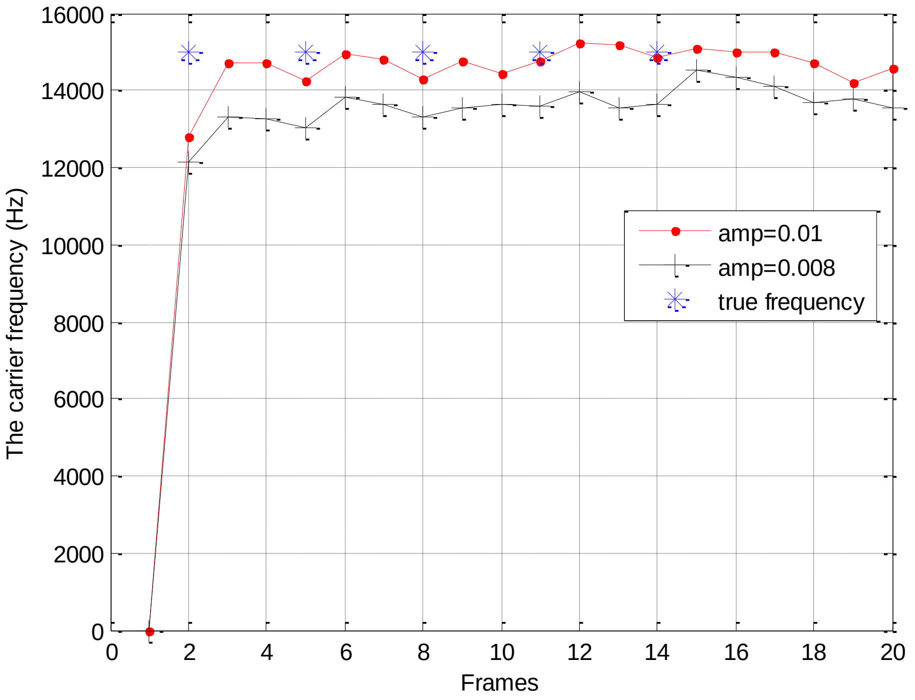

Figure 3.27 The average estimated carrier frequency over 50 simulations

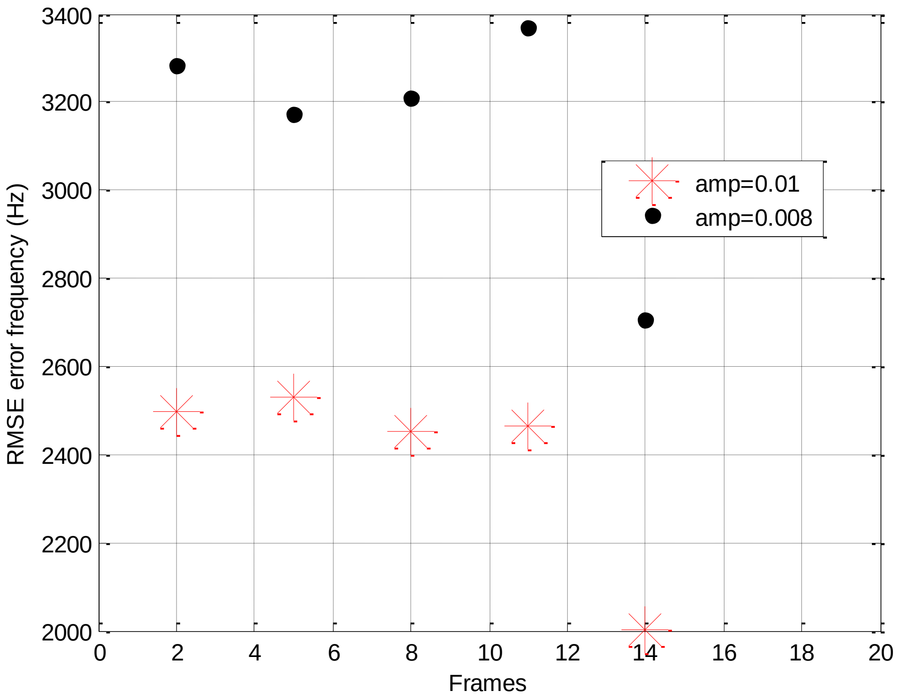

Figure 3.28 The RMS error in carrier frequency over 50 simulations

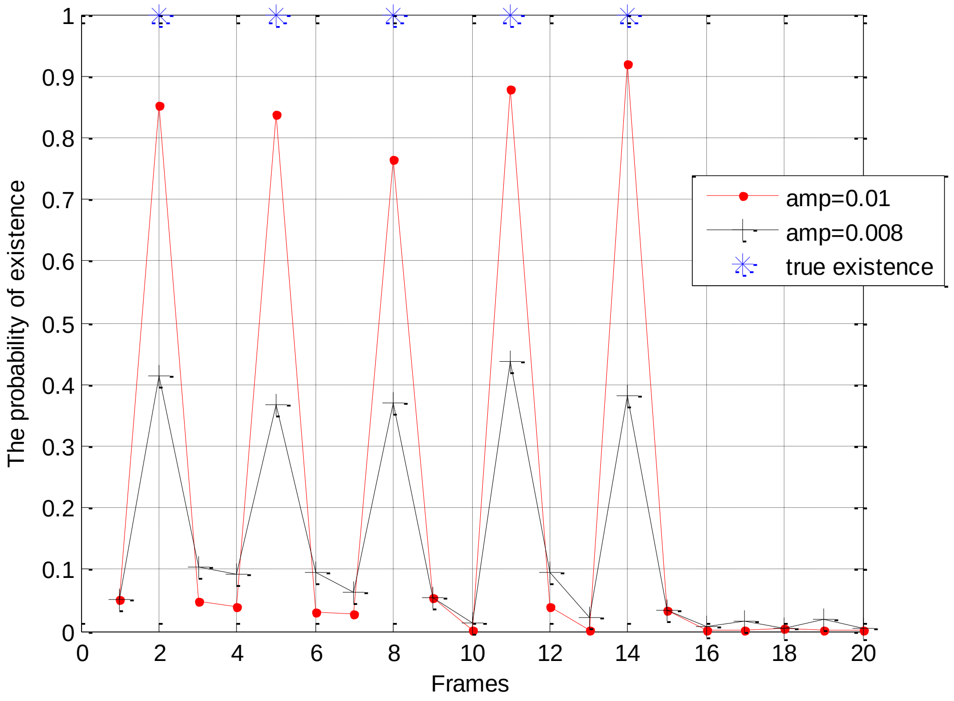

Figure 3.29 The average probability of existence over 50 simulations

The common parameters for the second set of experiments are given in Table 3.3. The pulse repetition interval (PRI) is 0.5sec and the carrier frequency f_c is 20kHz in this case, whereas in the first Monte Carlo Simulations these are 1.5sec and 15kHz respectively. The amplitude of the signal is changed in two sets. The signal amplitude is 0.01(peak SNR 9.79 dB) for the first set and 0.008 (peak SNR 7.85 dB) for the second set. 50 Monte Carlo runs are done for each set. The plots of the results are given in Figure 3.30, Figure 3.31 and Figure 3.32.

The average estimated carrier frequency and its corresponding RMS error are given in Figure 3.30 and Figure 3.31 respectively. These figures demonstrate that estimation of the carrier frequency calculated by the filter is consistent. However, the higher SNR provides lower RMS error and better estimated frequency.

The detection performance of the algorithm is shown in terms of the probability of existence in Figure 3.29. High probability of existence indicates the frames consisting pulses whereas the other frames which do not consist pulses have probability of existence values lower than 0.05.

Table 3.3 Monte Carlo Simulation Parameters(B)

The carrier frequency, f_c	$20kHz$
The pulse repetition interval, PRI	$0.5\sec$
The pulse width, PW	$20m\sec$
The variance of Gaussian Noise, $\sigma_w{}^2$	0.1
Peak SNR	9.79 dB , for signal amplitude=0.01 7.85 dB , for signal amplitude=0.008
Average SNR	-4.19 dB , for signal amplitude=0.01 -6.13 dB , for signal amplitude=0.008
Total Simulation Time	$10\sec$
Number of Frames (Data is divided into frames in time corresponding to $0.5\sec$)	20
Number Of Pulses in the Data	7 pulses at frame 4,5,6,7,8,9 and 10
The sampling frequency, f_s	$50kHz$
The initial probability of existence	0.05
The probability of birth, P_b	0.2
The probability of death, P_d	0.2
Number Of Particles	1000

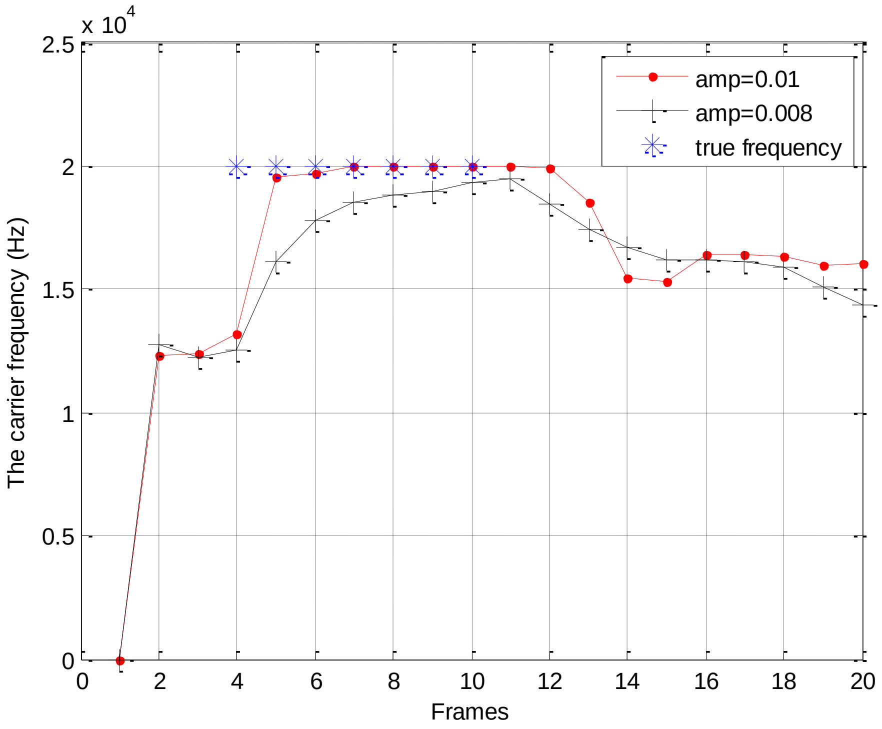

Figure 3.30 The average estimated carrier frequency over 50 simulations

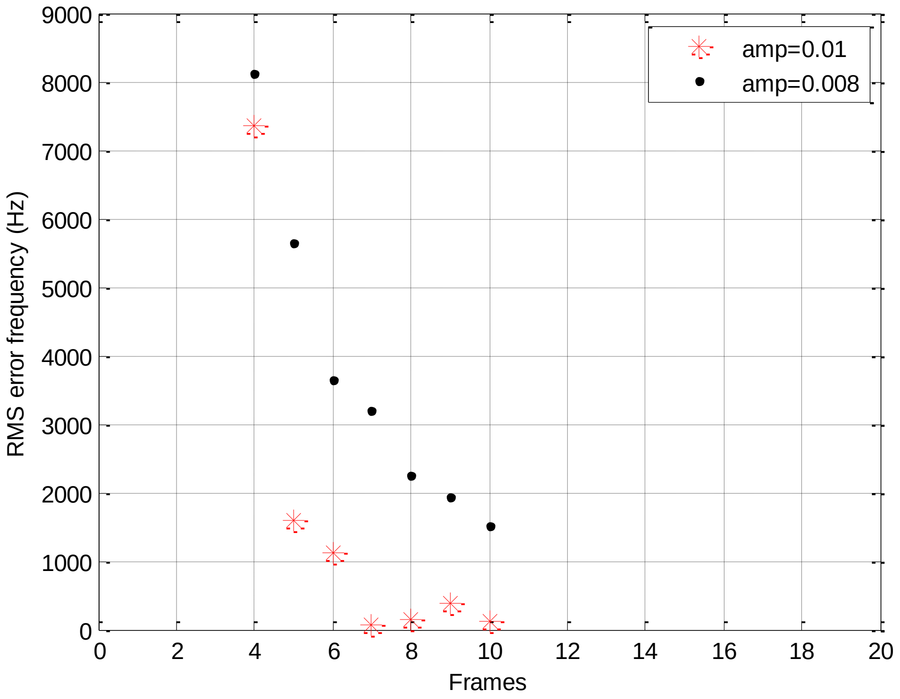

Figure 3.31 The RMS error in carrier frequency over 50 simulations

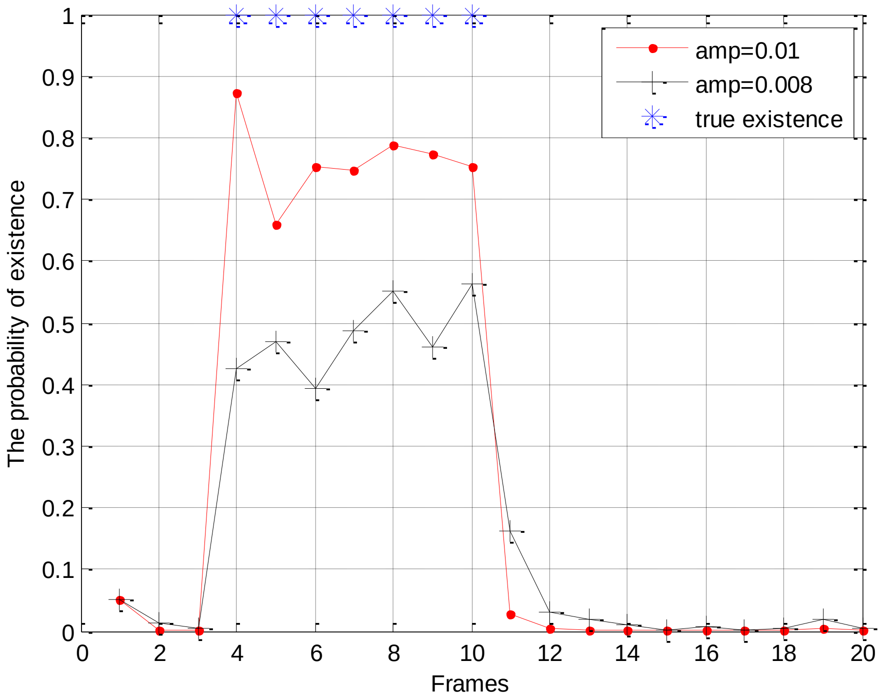

Figure 3.32 The average probability of existence over 50 simulations

3.9 *Conclusions*

In this chapter, the detection of low SNR signals with TBD concept is explained and the simulations that release the performance of the algorithm are done.

In section 3.7, the histogram of the particles vs. the carrier frequency component at frame 2, 5, 7, 11, 17 and the carrier frequency component vs. the weights of the particles are given in Figure 3.10 and Figure 3.11 for the first simulation, and for second simulation in Figure 3.18 and Figure 3.19. Figure 3.10 and Figure 3.11 show that in frame 2 the particles appear randomly dispersed in frequency but as the filter deduces from the data the presence and the frequency of the signal, the particle cloud becomes more concentrated around the true frequency. Besides this, the weights are higher for the particles whose frequency component is around the true frequency of the signal. The same observation is valid for Figure 3.18 and Figure 3.19.

The estimated frequency and the estimated arrival time of the pulses are given in Figure 3.12 and Figure 3.13 respectively for the first simulation. These figures show that there is a slight difference between the estimated frequency and the true frequency. Similarly, the arrival time of the pulses are estimated quite well. Figure 3.20 and Figure 3.21 give the estimated frequency and estimated arrival time of the pulses for the second simulation. The SNR is lower in this simulation therefore the performance of the filter in estimating the frequency and the arrival time of the pulses is degraded in this case, but it is still satisfactory.

The probabilities of existence vs. frames are given in Figure 3.14 and Figure 3.22 for first and second simulation respectively. As it is stated, the pulses exist at frames 2, 5, 8, 11 and 14 for both simulations. Figure 3.14 shows that the probability of existence is 1 for frames 2, 5, 8, 11 and 14. However, in Figure 3.22, the probability of existence is higher than 0.7 for frames 5, 8, 11 and 14 but it is lower than 0.1 at frame 2. It means that the filter could not detect the pulse at frame 2 since the amplitude is lower in the second simulation. Finally Figure 3.26 shows the estimated arrival time of the pulses. As it is seen, the arrival time of the pulses can be used to deduce the PRI of the signal.

In section 3.8, the performance of the algorithm is studied. 50 Monte Carlo simulations are done for each scenario and the results that reveal the performance of the developed algorithm are obtained. The scenario parameters are given in Table 3.2 and Table 3.3.

Figure 3.27 and Figure 3.28 show the performance of the algorithm in estimating the carrier frequency for the first scenario. The average estimated frequency over 50 simulations is given in Figure 3.27. In Figure 3.28, it is seen that the filter estimates the carrier frequency of the signal within a distance of 3500 Hz for the signal amplitude 0.008 (peak SNR 7.85 dB) and within a distance of 2500 Hz for amplitude 0.01 (peak SNR 9.79 dB). As it is expected, the error is lower when the SNR is higher.

The average probability of existence over 50 simulations is given in Figure 3.29. This figure demonstrates that the filter can detect the pulses even when the peak SNR is as low as 7.85 dB. The frames consisting pulses can be easily determined using this kind of figure.

Similarly, the filter performance for the second scenario can be investigated using Figure 3.30 and Figure 3.31. The average estimated frequency over 50 simulations is given in Figure 3.30. In Figure 3.31, it is seen that the error in estimating the carrier frequency of the signal is lower than 3500 Hz after frame 6 for amplitude 0.008 (peak SNR 7.85 dB) and it is lower than 1500 Hz after frame 5 for amplitude 0.01 (peak SNR 9.79 dB). As it is in the first case, the performance of the filter gets better when the SNR is higher. The average probability of existence over 50 simulations is given in Figure 3.32. As it is seen, low SNR signals with low duty cycle can be detected using this kind of approach.

CHAPTER 4

FURTHER ANALYSIS OF THE PERFORMANCE OF THE FILTER

4.1 *Introduction*

This chapter is devoted to the analysis of the performance of the proposed filter for changes in the carrier frequency and pulse repetition interval (PRI).

In the first part, the developed particle filter with TBD algorithm is used to detect the signals emitting from frequency agile systems. These systems change their operating frequency from burst-to-burst or from pulse-to-pulse basis. Frequency agility is preferred mainly because the system has a quite strong protection from jamming if it is frequency agile. Frequency agility forces the enemy to spread its available jamming power over a significantly increased bandwidth [18]. This means that effective jamming cannot be formed in the case of frequency agility.

New technologies in electronics make it possible for systems like radars or sonars utilize various PRIs. The filter performance when the emitting system is changing PRI is tested in the second experiment. Sonar uses low PRF when the target is far away and it increases the PRF when it gets closer. The reason behind this situation is the range ambiguity. Low PRF increases the unambiguous range of the system. However, when the target is close to the system, sonar increases the PRF to have more return signals.

4.2 *Simulations*

The scenario that the emitting system is frequency agile is tested in the first experiment. The common parameters of the Monte Carlo Simulations are given in Table 4.1. The simulated data is frequency agile from burst to burst. There are 5 pulses with carrier frequency 20 kHz appear at 1.6, 2.6, 3.6, 4.6, 5.6 seconds and there are 5 pulses with carrier frequency 10 kHz appear at 6.6, 7.6, 8.6, 9.6, 10.6 seconds. The signal in time domain is shown in Figure 4.1. Some of the measurement frames are given in Figure 4.2 when the SNR is 9.79 dB. The signal is circled in red in 12th and 14th frames. It is obvious that detecting the existence and the parameters of the signal visually is not possible even for SNR 9.79 dB case. The amplitude of the signal is changed in two sets. The signal amplitude is 0.01 (peak SNR 9.79 dB) for the first set and the amplitude is 0.008 (peak SNR 7.85 dB) for the second set. 50 Monte Carlo runs are done for each set. The plots of the results are given in Figure 4.3, Figure 4.4 and Figure 4.5.

The average estimated carrier frequency and its corresponding RMS error are given in Figure 4.3 and Figure 4.4 respectively. These figures show that consistent estimates of the carrier frequency are calculated by the filter in frequency agile conditions. With one frame delay, the estimated carrier frequency gives the consistent values in the case of the frequency change. However, the higher amplitude of the signal provides better estimated frequency and lower RMS errors.

The detection performance of the algorithm is shown in terms of the probability of existence in Figure 4.5. This figure can be used to determine the frames that have signal. As it is expected, the frames consisting pulses have high probability of existence whereas the other frames which do not consist pulses have probability of existence values lower than 0.15.

Table 4.1 Simulation Parameters for the First Experiment

The carrier frequency, f_c	$20kHz$, $10kHz$
The pulse repetition interval, PRI	$1\sec$
The pulse width, PW	$20m\sec$
The variance of Gaussian Noise, $\sigma_w{}^2$	0.1
Peak SNR	9.79 dB , for signal amplitude=0.01 7.85 dB , for signal amplitude=0.008
Average SNR	-7.20 dB , for signal amplitude=0.01 -9.14 dB , for signal amplitude=0.008
Total Simulation Time	$15\sec$
Number of Frames (Data is divided into frames in time corresponding to $0.5\sec$)	30
Number Of Pulses in the Data	5 pulses of $20kHz$ at frame 4,6,8,10,12 5 pulses of $10kHz$ at frame 14, 16, 18, 20, 22
Time Of Arrival (Pulses)	20kHz carrier frequency at 1.6, 2.6, 3.6, 4.6, 5.6 seconds 10kHz carrier frequency at 6.6,7.6,8.6,9.6,10.6 seconds
The sampling frequency, f_s	$50kHz$
The initial probability of existence	0.05
The probability of birth, P_b	0.2
The probability of death, P_d	0.2
Number Of Particles	1000

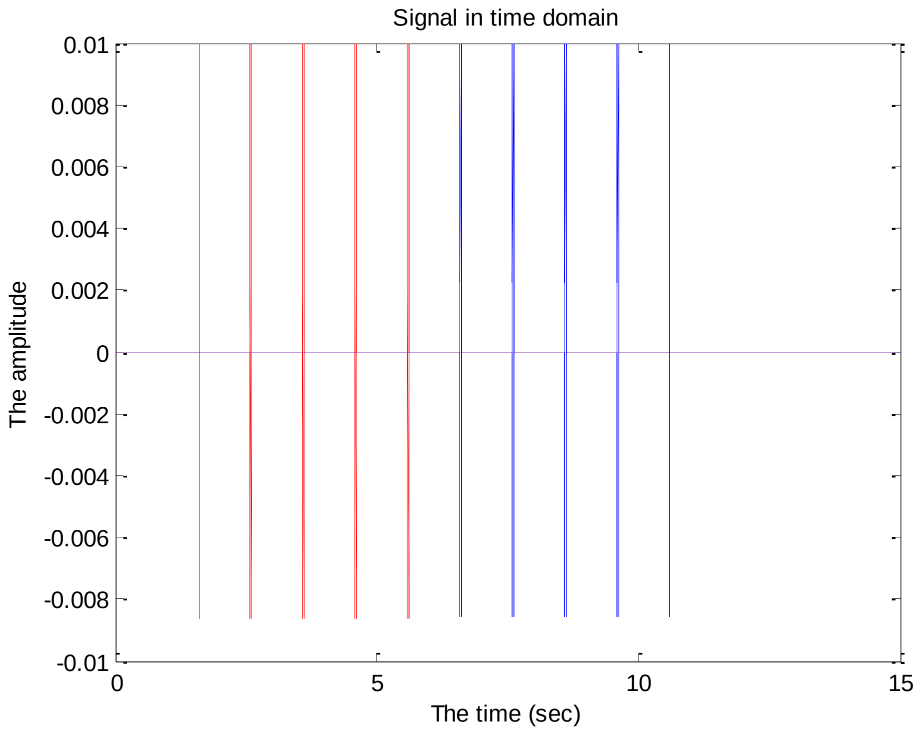

Figure 4.1 The signal in time domain, the amplitude is $amp = 0.01$, the carrier frequency $fc = 20kHz$ until time=6 sec and $fc = 10kHz$ after time=6.6 sec, the PRI $PRI = 1\sec$ and the pulse width $PW = 20\text{msec}$

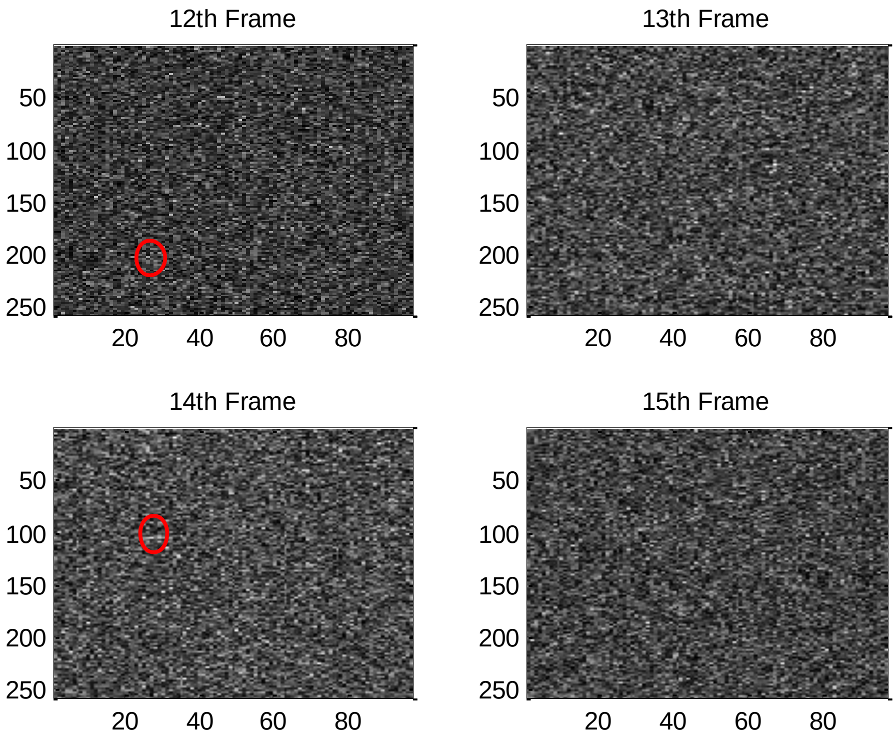

Figure 4.2 The measurement frames (peak SNR 9.79 dB)

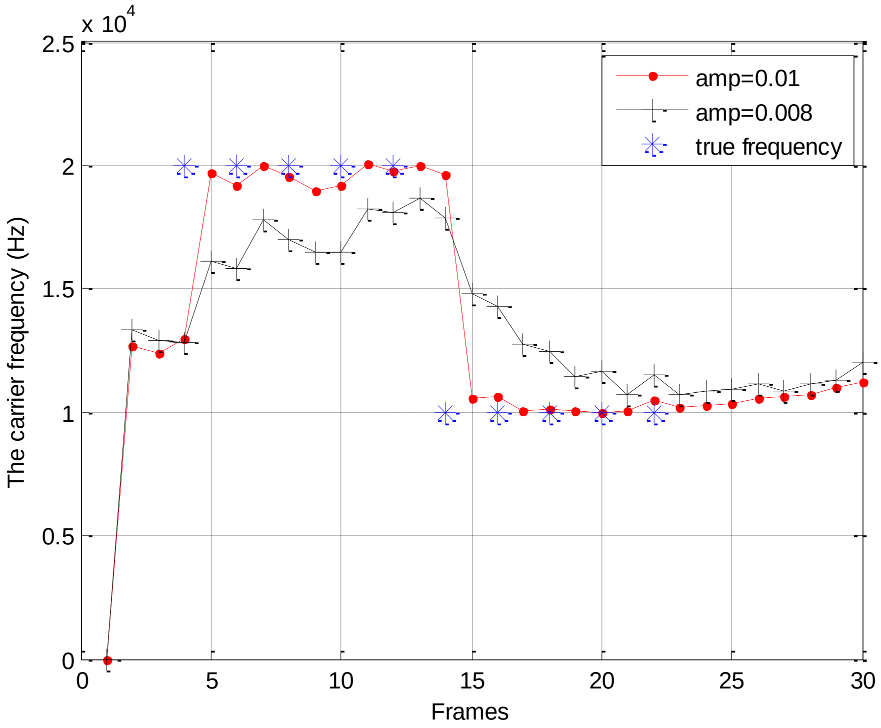

Figure 4.3 The average estimated carrier frequency over 50 simulations

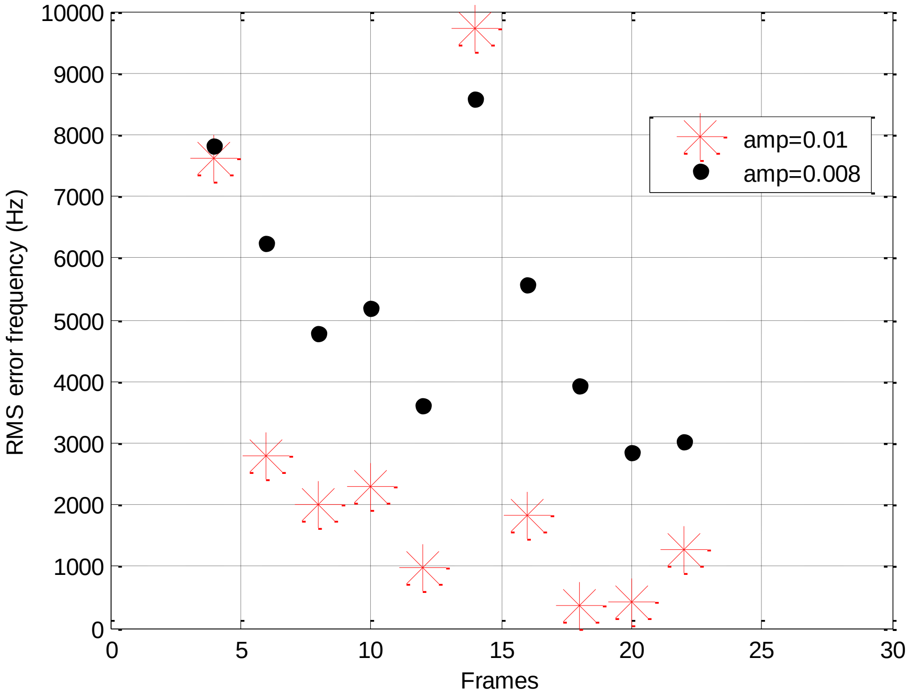

Figure 4.4 The RMS error in carrier frequency over 50 simulations

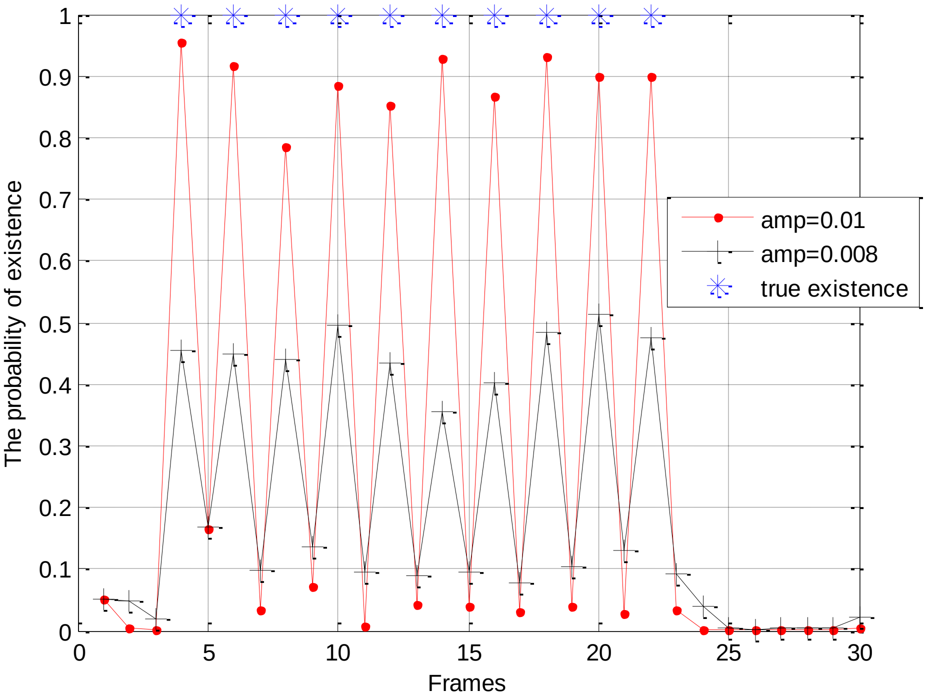

Figure 4.5 The average probability of existence over 50 simulations

The common parameters of the second scenario are given in Table 4.2. The simulated data is PRF agile, the pulse repetition interval changes from burst to burst. There are 5 pulses with pulse repetition interval $1.5\sec$ appear at 1.6, 3.1, 4.6, 6.1,7.6 seconds and there are 5 pulses with pulse repetition interval $2\sec$ appear at 9.6, 11.6, 13.6, 15.6, 17.6 seconds. The signal in time domain is shown in Figure 4.6. The 16th, 18th ,20th and 22nd measurement frames are given in Figure 4.7 when the peak SNR is 9.79 dB. There is signal in the 16th and 20th measurement frame circled in red, but there is only noise in the 18th and 22nd frames. As it is stated before, this figure shows that it is not possible to detect the existence of the signal visually for the SNR of 9.79 dB. Two experiments are conducted for two different SNR values. The signal amplitude is 0.01 (peak SNR 9.79 dB) for the first set of experiments and the amplitude is 0.008 (peak SNR 7.85 dB) for the second set. Each set is tested in 50 Monte Carlo runs. The plots of the results are given in Figure 4.8, Figure 4.9, Figure 4.10 and Figure 4.11.

Figure 4.8 and Figure 4.9 give the average estimated carrier frequency and the RMS error in frequency respectively. Even in PRF agile conditions, consistent estimates of the carrier frequency are given by the filter. The accuracy of the estimated carrier frequency gets better at the frame which is one after the occurrence of the signal. This is reasonable since the filter corrects itself after getting the measurement. Besides, higher SNR increases the performance of the filter.

A change in the PRI reduces performance of the signal existence at the point of PRI change. However this reduction is not severe and a robust threshold is still possible.

The PRI of the data can be deduced from Figure 4.11. It is stated that data is divided into frames in time corresponding to $0.5\sec$, the time difference between two consecutive frames in which the probability of existence is high give the PRI of the data. As it is seen in the figure, the pulses exist at frames 4, 7, 10, 13, and 16.

There are 3 frames between two consecutive pulses and that corresponds to $1.5\sec$.It is obtained that the PRI is $1.5\sec$ up to frame 16. Similarly the pulses existing at frames 16, 20, 24, 28, 32, and 36 give a PRI value of $2\sec$.

Table 4.2 Simulation Parameters for the Second Experiment

The carrier frequency, f_c	$20kHz$
The pulse repetition interval, PRI	$1.5\sec$, $2\sec$
The pulse width, PW	$20m\sec$
The variance of Gaussian Noise, $\sigma_w{}^2$	0.1
Peak SNR	9.79 dB , for signal amplitude=0.01 7.85 dB , for signal amplitude=0.008
Average SNR	-8.96 dB , for signal amplitude=0.01 when PRI is 1.5 sec -10.21 dB , for signal amplitude=0.01 when PRI is 2 sec -10.90 dB , for signal amplitude=0.008 when PRI is 1.5 sec -12.15 dB , for signal amplitude=0.008 when PRI is 2 sec
Total Simulation Time	$20\sec$
Number of Frames (Data is divided into frames in time corresponding to $0.5\sec$)	40
Number Of Pulses in the Data	5 pulses of $20kHz$ at frame 4, 7, 10, 13, 16 with PRF $1.5\sec$ 5 pulses of $20kHz$ at frame 20, 24, 28, 32, 36 with PRF $2\sec$
Time Of Arrival (Pulses)	20kHz carrier frequency at 1.6, 3.1, 4.6, 6.1,7.6 seconds 20kHz carrier frequency at 9.6, 11.6, 13.6, 15.6, 17.6 seconds
The sampling frequency, f_s	$50kHz$
The initial probability of existence	0.05
The probability of birth, P_b	0.2
The probability of death, P_d	0.2
Number Of Particles	1000

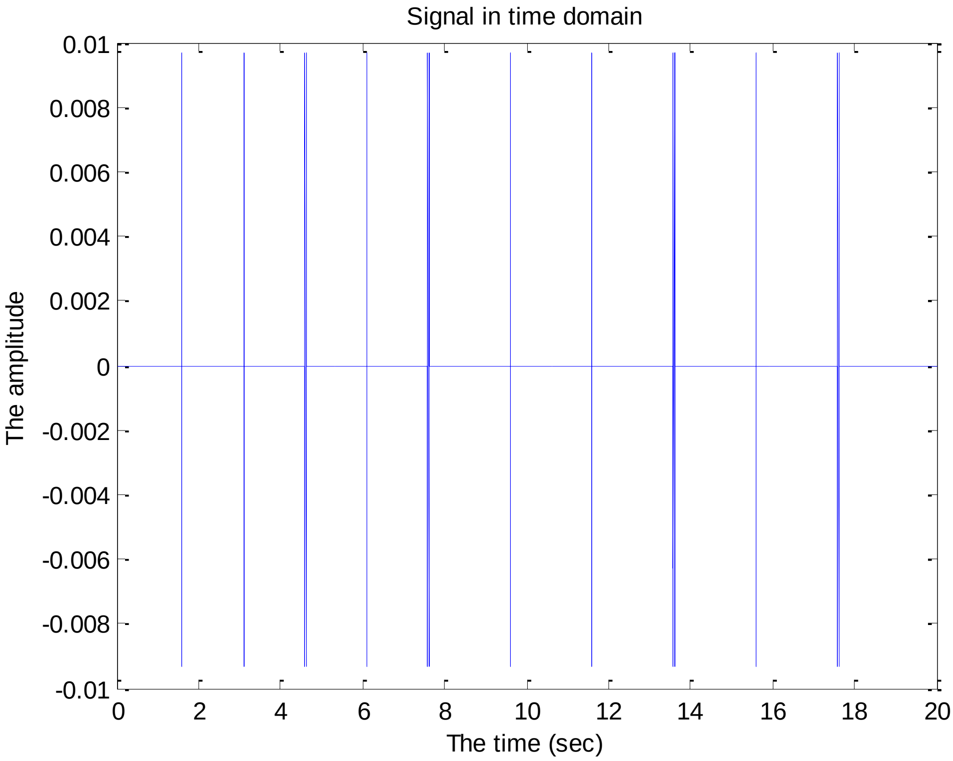

Figure 4.6 The signal in time domain, the carrier frequency $fc = 20kHz$, the PRI $PRI = 1.5\sec$ until time=8sec and the $PRI = 2\sec$ until time=18sec

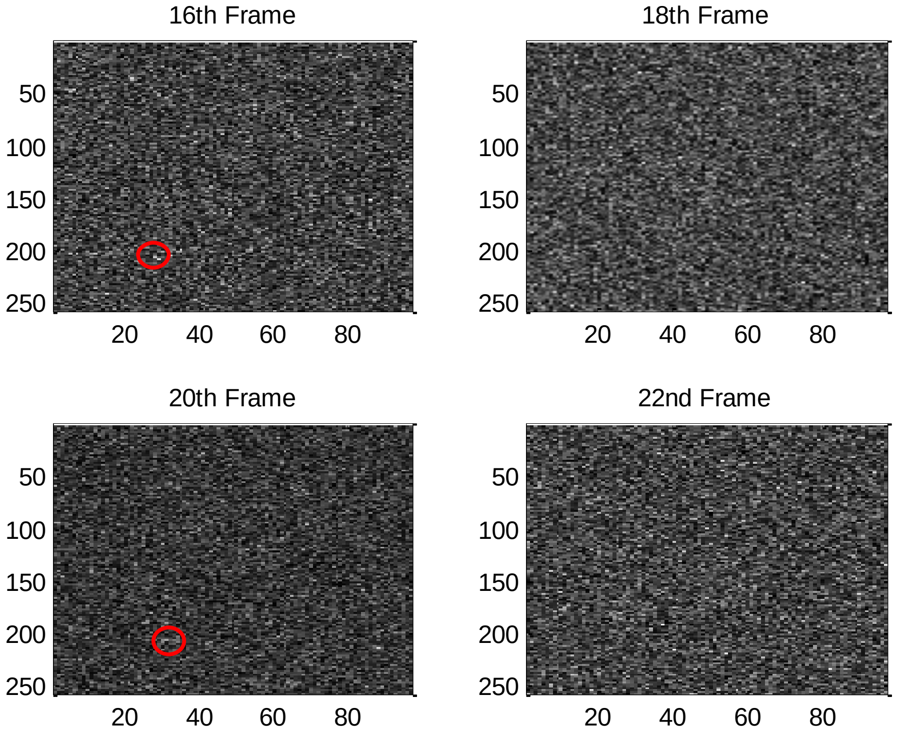

Figure 4.7 The measurement frames (peak SNR 9.79 dB)

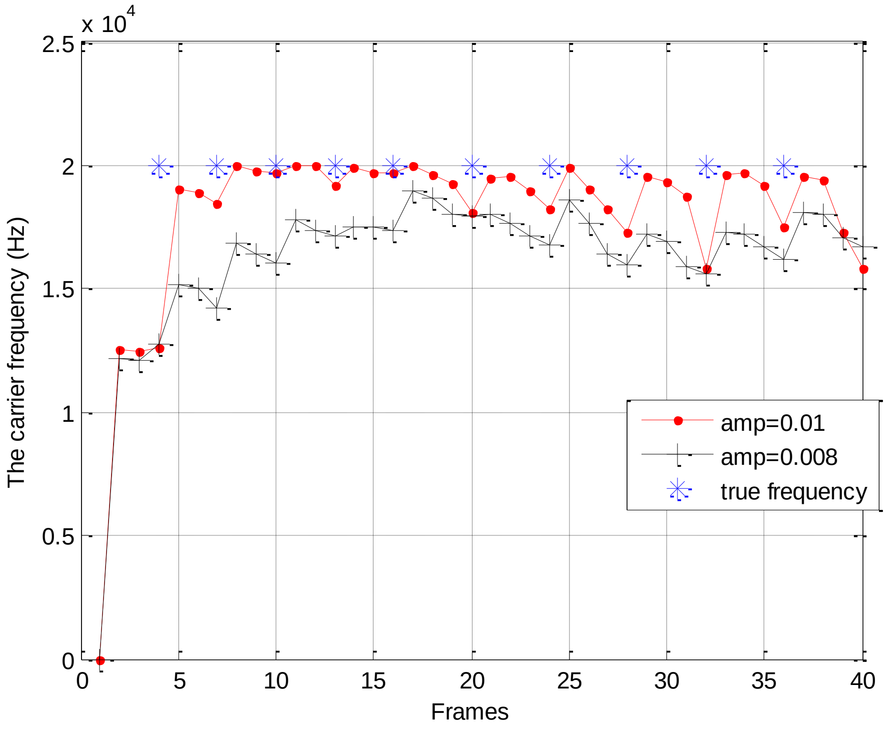

Figure 4.8 The average estimated carrier frequency over 50 simulations

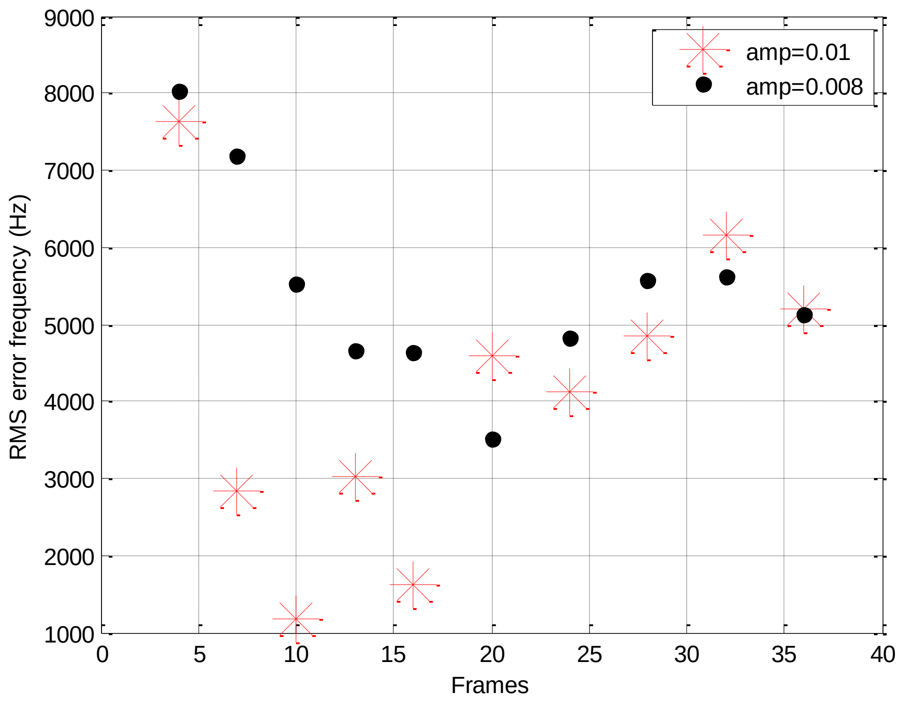

Figure 4.9 RMS error in carrier frequency over 50 simulations

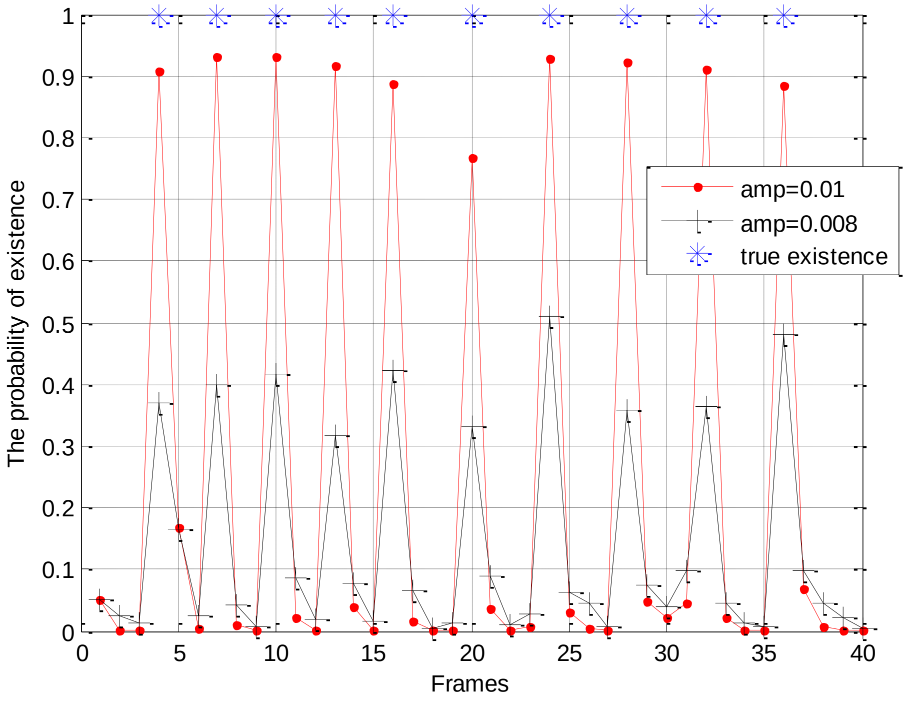

Figure 4.10 The average probability of existence over 50 simulations

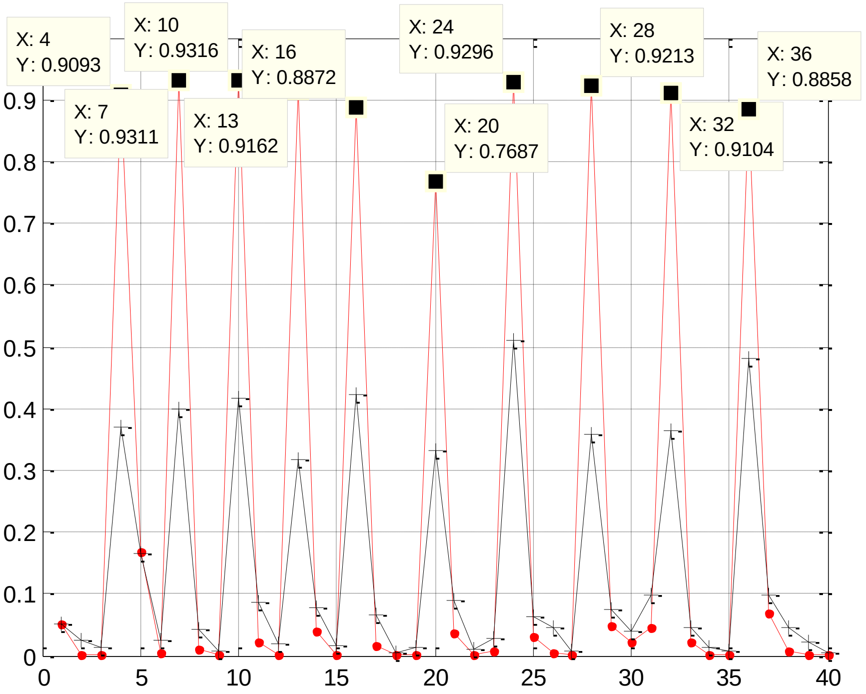

Figure 4.11 The plot which demonstrates that PRI can be deduced from the probability of existence data

4.3 *Conclusions*

In the first set of experiments, 50 Monte Carlo simulations are done for the scenario in which the emitter system is frequency agile from burst to burst; there are 5 pulses with carrier frequency 20 kHz and following 5 pulses with carrier frequency 10 kHz. The results demonstrate the performance of the developed algorithm.

Figure 4.3 and Figure 4.4 show the performance of the algorithm in estimating the carrier frequency. The average estimated frequency over 50 simulations is given in Figure 4.3. The filter estimates of frequency given in the figures should be interpreted with a delay of one frame. If the average estimated frequency for amplitude 0.01 (peak SNR 9.79 dB) and 0.008 (peak SNR 7.85 dB) are compared, it is clear that the estimation performance of the algorithm gets better as the amplitude of the signal is higher. In Figure 4.4, as it is expected, the error is higher when the carrier frequency of the signal changes from 20 kHz to 10 kHz. The average probability of existence over 50 simulations is given in Figure 4.5. This figure demonstrates that the filter can detect the pulses even when the SNR is as low as 7.85 dB. The frames consisting pulses can be easily determined using this result by thresholding the existence probability.

The second set of experiments reveal the performance of the algorithm when the system which changes the pulse repetition frequency (PRF). In the scenario, there are 5 pulses with pulse repetition interval of $1.5\sec$ that are followed with 5 pulses with PRI of $2\sec$.

From Figure 4.8 and Figure 4.9, it is seen that the RMS error is higher in frames where the PRI is $2\sec$ compared to frames in which PRI is $1.5\sec$. This situation is reasonable since there are 3 frames between two consecutive pulses if PRI is $1.5\sec$; however, there are 4 frames in the other case. The smaller duty cycle causes the importance weights corresponding to the true frequency in the particle filter to decay.

The average probability of existence over 50 simulations is given in Figure 4.10. This figure shows that the filter can detect the pulses even when the SNR is as low as 7.85 dB. When the amplitude is 0.01, the probability of existence is lower in frame 20 compared to other frames that contain pulses which is reasonable since the system changes its PRI at that frame. Nevertheless, the frames consisting pulses can be determined.

CHAPTER 5

CONCLUSIONS

The real focus of this thesis is on the particle filter application of the track-before-detect (TBD) approach to sonar signals. In Chapter 2, the theoretical background of the particle filter is given and the related works in the literature about TBD approach are briefly explained.

In Chapter 3, a new particle filter which aims to detect and track pulsed modulated sinusoidal signals in noisy environment is developed. Detection of low SNR signals is a challenging problem. The conventional methods use thresholding, however; low SNR signals require a low threshold and this results a high rate of false detections; following that the tracking system form false tracks. The proposed solution is a recursive, Bayesian track-before-detect filter implemented using particle-based methods. As it is seen in the experiments, detecting the existence of the signal and finding and tracking the parameters of it is not possible for the cases considered in this thesis visually. The simulations show that the algorithm presented in this thesis can detect signals which cannot be detected by conventional methods. Besides detection, the tracking performance of the filter is satisfying. The proposed filter estimates the carrier frequency and PRI of the signal.

The originality of this work is the model developed. Although there are recently developed methods in the literature to track low SNR video signals, our problem has some inherent differences compared with the low SNR video tracking problem. One of the main differences is the existence of the signal only at some frames in a periodic fashion. This requires an original definition of the output. The model is flexible enough to accept prior information about the unknown parameters as prior density functions. This flexibility is used in PRI prior. The same technique can (should) be applied to the selection of carrier frequency as well.

The parameters of the signal are estimated using the MMSE estimation in this work. As a future work, the other estimation methods such as maximum a posteriori can be applied and the performance of the different estimation methods can be compared.

In Chapter 4, the systems that employ frequency agility and PRF agility are considered. The simulations demonstrate that the filter estimates the true carrier frequency with one frame delay under frequency agility from burst to burst conditions. It should be noted that the detection performance is not degraded under the frequency agility conditions. Besides, the PRI of the signal can be deduced under PRF agility scenarios. The detection performance is not degraded, however it is seen that the tracking performance improves when the number of frames between two consecutive pulses decrease.

REFERENCES

[1] Poor, H., *Introduction to Signal Detection and Estimation,* Springer-Verlag, 1994.

[2] Ristic, B., Arulampalam, S., and Gordon, N., *Beyond the Kalman Filter: Particle Filters for Tracking Applications,* Artech House, 2004.

[3] Doucet, A., Godsill, S., and Andrieu, C., “On sequential Monte Carlo sampling methods for Bayesian filtering,” *Statistics and Computing,* vol. 10, no. 3, pp. 197–208, 2000.

[4] Papoulis, A. and Pillai, S., *Probability, random variables and stochastic processes,* McGraw Hill, 2002.

[5] Murphy K.P., Markov Chain Monte Carlo (MCMC), 3 November 2006.

[6] Blackman, S., Popoli, R., *Design and Analysis of Modern Tracking Systems,* Norwood, MA: Artech House, 1999.

[7] Barniv, Y., “Dynamic programming solution for detecting dim moving targets,” *IEEE Trans. Aerospace and Electronic Systems,* vol. 21, pp. 144–156, 1985.

[8] Carlson B., E. Evans, S. Wilson, “Search Radar Detection and Track with the Hough Transform, part I: System concept”, *IEEE Trans. Aerospace and Electronic Systems,* vol. 30, pp. 102-108, January 1994.

[9] Stone, L. D., Corwin, T. L., Barlow, C.A., *Bayesian Multiple Target Tracking,* Artech House, Inc., Norwood, MA, 1999.

[10] Driessen, H., Boers, Y., "An efficient particle filter for non-linear jump Markov systems," in Proceedings of the IEE Seminar on Target Tracking: Algorithms and Applications, Sussex, UK, March 2004.

[11] Rutten, M. G., Gordon, N. J., and Maskell, S., "Recursive track-before-detect with target amplitude fluctuations," *IEE Proceedings on Radar, Sonar and Navigation,* vol. 152, no. 5, pp. 345-352, 2005.

[12] Streit, R. L., "Tracking on intensity-modulated data streams," Tech. Rep. 11221, NUWC, Newport, RI, USA, May 2000.

[13] Streit, R. L., Graham, M. L., and Walsh, M. J., "Multitarget tracking of distributed targets using histogram-PMHT," *Digital Signal Processing,* vol. 12, no. 2-3, pp. 394-404, 2002.

[14] Davey, S. J., Rutten, M. G., and Cheung, B., “A Comparison of Detection Performance for Several Track-before-Detect Algorithms”, *EURASIP Journal on Advances in Signal Processing,* Volume 2008.

[15] Polmar, N. "The U. S. Navy Electronic Warfare (Part 1)" *United States Naval Institute Proceedings,* p.137, October 1979.

[16] Skolnik, M.I., *Introduction to Radar Systems,* McGraw-Hill, 3rd Edn., 2001.

[17] Rutten, M.G., Ristic, B., Gordon, N., “A Comparison of Particle Filters for Recursive Track-before-Detect”, in 7th International conference on Fusion, 2005.

[18] Van Brunt, L.B., *Applied ECM,* Volume 2, EW Engineering Inc., 1982.

[19] Mahafza, B.R., *Radar Systems Analysis and Design Using Matlab,* Chapman & Hall/CRC, 2000.

[20] Chen, V.C., Ling, H., *Time-Frequency Transforms for Radar and Signal Analysis,* Artech House, Inc. 2002.